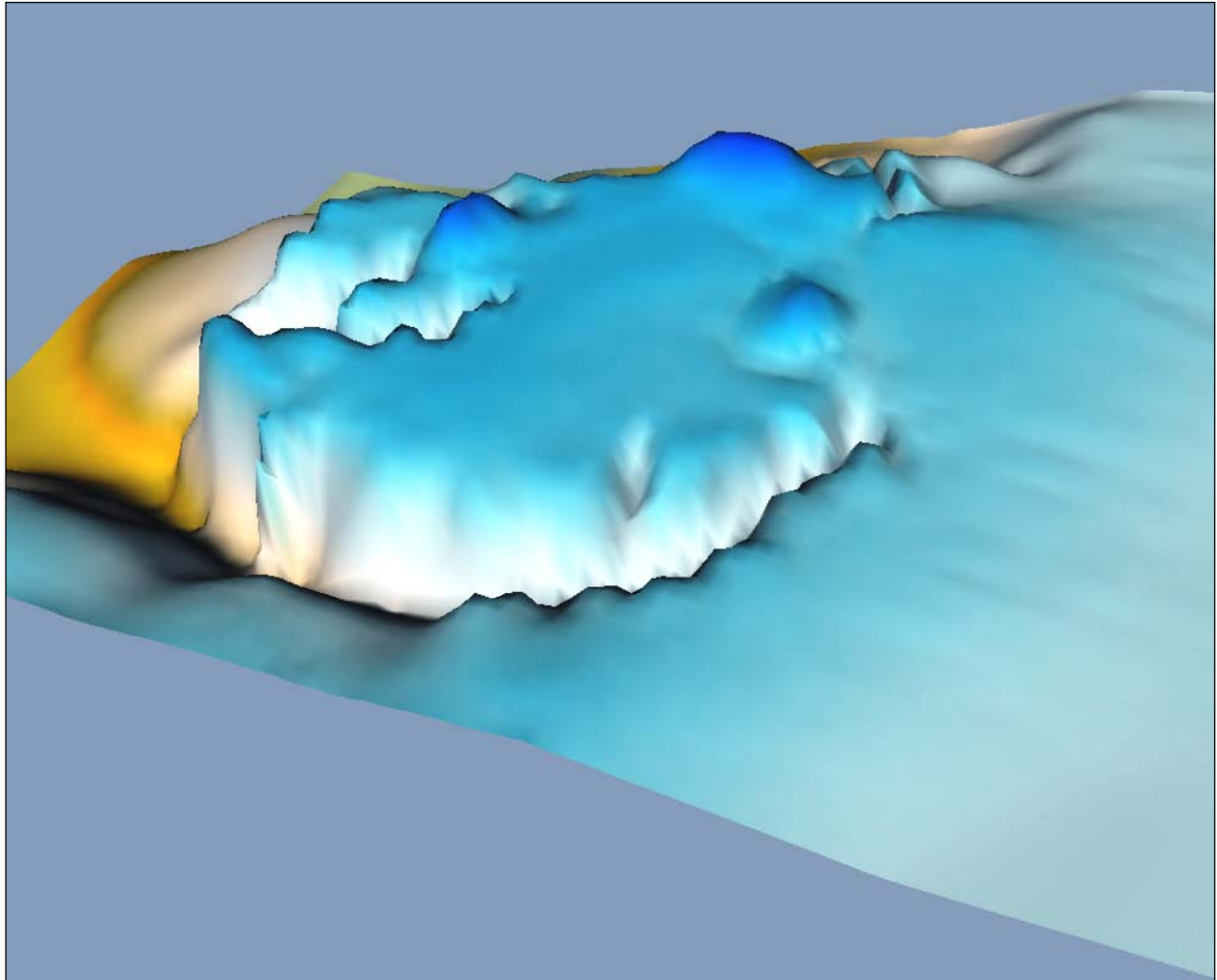


Geophysical Investigations at Feltus Mounds (22Je568), Jefferson County, MS.



By:

Edward R. Henry and Jay K. Johnson

**Center for Archaeological Research
Department of Sociology and Anthropology**



The University of Mississippi

Geophysical Investigations at Feltus Mounds (22Je568), Jefferson County, MS.

By:

Edward R. Henry and Jay K. Johnson

Report Prepared For:

Mississippi Department of Archives and History

P.O. Box 571

Jackson, MS 39205-0571

Phone: 601-576-6940

Fax: 601-576-6955

Contact:

Pamela Edwards Lieb

plieb@mdah.state.ms.us

Report Submitted By:

Edward R. Henry

Center for Archaeological Research

Department of Sociology and Anthropology

106 Leavell Hall

University of Mississippi

University, MS 38677

2012



Edward R. Henry
Principal Investigator

ACKNOWLEDGEMENTS

The author would like to thank Pamela Edwards Lieb and the Mississippi Department of Archives and History for making available the funding under which this work was completed. Dr. Vin Steponaitis, John O’Hear, Megan Kassabaum, Erin Nelson, and David Cranford, as well as members of the 2012 University of North Carolina summer field school in archaeology proved invaluable throughout the project; constantly providing background and knowledge of the Feltus Mounds site. Jay Johnson provided very helpful comments on previous drafts of this report.

INTRODUCTION

In May of 2012, Edward R. Henry conducted a multi-instrument geophysical investigation at the Feltus Mounds site (22Je568), a Coles Creek-phase site in southwest Mississippi (Figure 1). The eastern and southern flanks of Mound A, and the top and eastern flank of Mound B were covered during the project (Figure 2). A dataset was collected on Mound C by students in the University of North Carolina-Chapel Hill (UNC-CH) field school. Their results will be discussed here. Fundamentally, this research intended to employ various geophysical techniques to locate and map subsurface archaeological features that had previously been encountered at the site (i.e. clay floors, pits, midden, etc.) and to assess the nature of mound construction through an investigation of stratigraphy. Geophysical investigations were carried out in two stages during fieldwork, and included the use of magnetic gradiometry, ground-penetrating radar (GPR), electrical resistivity tomography (ERT), and down-hole magnetic susceptibility. After data from these instruments were processed, specific anomalies identified in the data were compared to known archaeological features and stratigraphy at the site.

Results of this investigation indicate that clay floors, and pit features comprise internal mound stratigraphy within Mound A. One possible unknown floor was mapped with the down-hole beneath the summit of Mound A. Investigations on Mound B found signatures that correspond to burials and prepared clay floors within the mound. Further, investigations here supported an interpretation that Mound B began as a low-wide platform. A similar interpretation is made based on down-hole data from Mound C.

GEOPHYSICAL METHODOLOGY

Geophysical surveys focus on detecting and documenting subsurface variation. Geophysical prospection methods were initially developed for the study of geological phenomena. However, in recent decades they have become more and more important for the detection of archaeological features (Clark 1996, Gaffney and Gater 2003, Johnson 2006, Smekalova et al. 2005). Geophysical technology was first applied to archaeology in Europe, and refined in and around Great Britain during the last half of the twentieth century (Clark 1996:11). Though geophysical technology has been applied to archaeological research in North America as a method of prospection since the 1930s (Aitken 1961), it was not until the 1970s that it became commonly used (Bevan 1975; Bevan and Kenyon 1975; Johnson 2006:9). During the 1980s, geophysical surveys in archaeology intensified as commercial equipment and software became more readily available, a trend that continues today. The increasing availability of commercial equipment has amplified the quality and quantity of data collected.

Most recently, archaeologists have begun to go beyond using geophysical technologies as a mere prospection tool focused on finding targets for excavation. Geophysical datasets are now beginning to be used in the creation and testing of archaeological and anthropological hypotheses at various scales of investigation (Conyers and Leckebusch 2010, Henry 2011, King et al. 2011,



Figure 1. Location of Feltus Mounds, on portions of the Chamblee, Church Hill, Pine Ridge, and Rodney USGS Quad Sheets. Map by the authors.

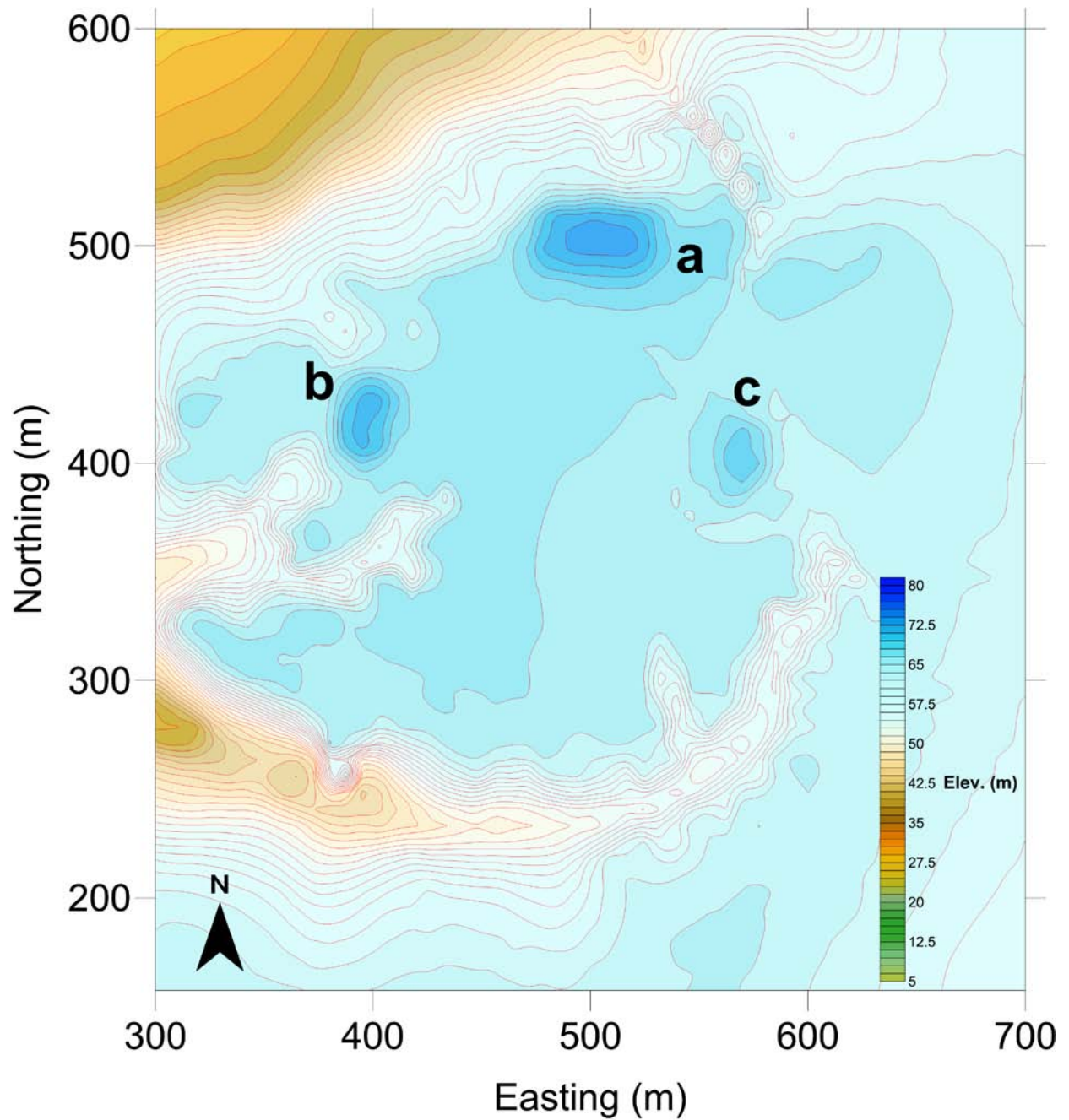


Figure 2. Topographic map of the Feltus Mounds site with extant mounds labeled. Contours exhibit 1.5 meter elevation changes. Map by the authors.

Kvamme 2003, McKinnon 2009, Thompson and Pluckhahn 2010, Thompson et al. 2011). These new uses of geophysical techniques in archaeology will certainly progress as more archaeologists utilize the technology. This research demonstrates how geophysics can help assess site structure and organization in mound construction when interpreted with a consideration of site stratigraphy.

MAGNETIC GRADIENT

A fluxgate gradiometer was used during the survey of Mound B at Feltus. These instruments are composed of two primary cores made of ferro-magnetic alloys wound in opposing directions, and a secondary coil that encompasses the primary coils to create a resultant zero magnetic flux (Aspinall et al. 2008:34). These coils are typically oriented one above the other at a set distance. The reading given by the gradiometer is then determined by calculating the difference between the two coils (Aspinall et al. 2008:40). Fluxgate gradiometers have become one of the most commonly utilized geophysical techniques in Britain and the United States (Clark 1996:68).

Gradiometers measure variations in the Earth's naturally occurring magnetic field, with data expressed in nanoteslas (nT) (Clark 1996:64, 69). They are considered passive geophysical instruments because they do not create or induce any artificial field into the ground in order to take a measurement (Aspinall et al. 2008:206). Gradiometers can detect two types of magnetism: thermoremanent (or remnant) and induced.

Archaeological features often exhibit high remnant magnetization because of thermal alteration to their ferrous mineral content. Aspinall et al. (2008:21) note that ferrous minerals (i.e., hematite, magnetite, and maghemite) found in naturally occurring clays exhibit extreme remnant magnetization when they are heated above their Curie temperatures (575-675 degrees Celsius). Detecting features with high remnant magnetism is possible because ferrous minerals that are naturally aligned in a random manner realign to Earth's magnetic field once heated above their Curie temperatures (Reynolds 2002:16). A gradiometer measures the impact that this locally magnetized field has on the Earth's natural magnetic field. Brick kilns, prepared hearths, and wattle-and-dab structures destroyed by fire are good examples of thermoremanent magnetic features.

Induced magnetism refers to the contrasts of a specific material's (mostly iron oxides) magnetic susceptibility in comparison to its surroundings (Aspinall et al. 2008:22). The three most important iron oxides found to usually affect induced magnetism are hematite, magnetite, and maghemite (Kvamme 2006:208). Induced magnetism is often closely related to long-term human occupation (Clark 1996:99). Human activities that can create induced magnetism and enhance the magnetic susceptibility of a matrix (i.e., soil), include burning vegetation, which causes oxygen reduction in topsoil and can reduce hematite to magnetite; the accumulation of organic waste that causes an increase of bacteria which can also create a reducing atmosphere for magnetic minerals called mineral fermentation; and the discarding of magnetic materials, such as fragmented ceramics and brick on the ground surface, which quickly make their way into the topsoil (Aspinall et al. 2008:24-25). Examples of induced magnetic features include burned surfaces, midden pits and privies, buried A soil horizons, and human living surfaces.

Interpreting gradiometer data begins by identifying anomalies, which may have high and low magnetic gradient values (Bevan 1998:23). Metal objects can be easily identified by their shape and strength of reading. Anomalies with strong narrowly spaced dipoles, or strong monopoles, are usually produced by ferrous material. Determining the depth below surface of a magnetic gradient target is hard to discern from magnetic gradient data. In some cases, a half-width rule can be used to estimate the depth of an anomaly. This rule depends on the drop-off of readings over the anomaly and assumes the buried material relating to the anomaly is simple and regular in shape (Bevan 1998:25). With the exception of buried iron targets, this technique is not often useful for archaeological geophysicists.

GROUND-PENETRATING RADAR

Ground-penetrating radar (GPR) is a geophysical method that utilizes electromagnetic energy to measure the differential reflection properties of subsurface soil strata (Conyers and Goodman 1997). This energy, transmitted as a radar wave, is sent into the ground to reflect off buried discontinuities (e.g., rocks, architecture, graves, and pits). Measuring the rate of reflection in a study area allows a GPR user to search for anomalies within a given area of interest (Conyers 2004).

When active, electromagnetic pulses are transmitted from a control unit. The pulses then propagate waves that penetrate the ground. The rate of time it takes for the wave to travel into the ground and reflect off a buried anomaly is measured and recorded by the GPR instrument (Conyers and Goodman 1997). A portion of the wave will continue further into the ground and continue to reflect off of discontinuities until finally the wave attenuates (the amplitude and/or intensity is too small to reflect back to the antenna). Electromagnetic properties within the soil, described here as relative dielectric permittivity (RDP, or the dielectric constant), can dramatically influence the depth and attenuation rate of radar waves. RDP is the ability of a material to store and pass an electromagnetic field. RDP, usually denoted by K , ranges from 1 for air to 81 for water and is expressed by $K = (C/V)^2$, where C is the velocity of light and V is the velocity of the radar wave traveling through a matrix (e.g., soil, rock, ice, or water) (Conyers 2004:48-49). High clay or salt content in soil, as well as water saturation (poorly-drained soil or subsurface water-pooling), can result in poor GPR survey results.

ELECTRICAL RESISTIVITY TOMOGRAPHY

Electrical resistivity tomography (ERT) is not commonly used in archaeological contexts. This geophysical technique is more commonly applied in the investigation of dams and levees, the detection of caves and tunnels, in the mapping of subsurface contamination plumes, for locating ground water aquifers, and determining depth to bedrock. However, ERT has been successfully applied in archaeological contexts across Europe to explore the internal contrasts of burial mounds, buried buildings, and barrows (Astin et al. 2007, Nuzzo et al. 2009, Tonkov and Loke 2006).

Electrical resistivity tomography is a geophysical method that measures the electrical properties of the earth's subsurface. Electrical resistivity (ρ) is a measurement of how strongly a

material resists the flow of an electric current introduced into the ground. Resistivity is considered a material property that varies from one material to the next. Since the artificially injected electrical current flows through the pore space of soils, geological parameters such as porosity, degree of saturation, pore water resistivity, and clay content ultimately affect electrical resistivity measurements. These parameters can be inserted into empirical equations (Archie's Law, Waxman-Smits equation) to estimate subsurface resistivity (Mavko, Mukerji, and Dvorkin 1998:282-287). Specifically, Archie's Law calculates an estimation of the resistivity of clean sands and rocks, while the Waxman-Smits equation predicts resistivity of soils where clay content is present.

ERT systems are generally comprised of a resistivity meter (source) that applies current to the earth via electrode switch cables and stainless steel electrodes. Electrode stakes are placed in the ground and arranged in a particular geometrical orientation (array type). The electrical current is injected through the electrodes, allowing the corresponding potential difference to be measured across the potential electrodes. The measurements that are recorded on the meter are the apparent resistivity, a calculation of the known injected current, measured potential difference, and electrode geometrical factor, which is based on the electrode position. Apparent resistivity values are not the "true resistivity" of the subsurface but can be used to build a 2D pseudosection that provides information on the distribution of electrical resistivity in the ground, depicted in Ohm-meters (Ohm-m). The survey file can later be transferred from the resistivity meter to an office computer/laptop and further processed and analyzed using imaging software.

DOWN-HOLE MAGNETIC SUSCEPTIBILITY

Down-hole magnetic susceptibility is one of the newer geophysical instruments developed specifically for, and used in, archaeology (Dalan 2001). The instrument consists of a small sensor that is lowered down 2.2 cm diameter core holes removed with an Oakfield-like push-tube soil corer. The down-hole technique measures volume magnetic susceptibility (κ) as expressed in SI units to a maximum depth of 3 m below ground surface. (Dalan 2006:162). The same induced magnetic features that can be detected with the in-phase component of an EM signal (i.e. burned surfaces, midden pits, mound stages and buried A soil horizons, as well as village living surfaces) can be detected with the down-hole system. However, the down-hole method succeeds in detecting these features at a much greater depth than surface-scanning EM instruments.

FIELD PARAMETERS

Fieldwork was conducted over two weeks in May 2012. Magnetic gradient data were collected with a single sensor of the Bartington Instruments, Inc. Grad 601-2 dual fluxgate gradiometer (Figure 3). Readings were collected at the .01 nT level every .25 cm along transects spaced 50 cm apart. Data were downloaded and processed in Geoscan Research's Geoplot 3.0 software package and then exported for visualization in Golden Software's Surfer 10 mapping program.



Figure 3. Edward Henry collecting gradiometer data with a single-sensor Bartington Instruments, Inc. Grad-601-2. Photograph by David Cranford.

GPR data were collected using a Geophysical Survey Systems, Inc. (GSSI) SIR-3000 with a 400 and 270 MHz shielded antenna. A survey wheel was used with these antennas to accurately record its position along each transect line (Figure 4). With the 400 MHz antenna, data were collected at 32 scans per meter and digitized to 512 samples per scan along transects separated by .5 m. The time window was set to 65 nanoseconds (ns) resulting in a maximum depth penetration of 2.45 m below surface in the local soil conditions. Data with the 270 MHz antenna were collected at 32 scans per meter and digitized to 512 samples per scan along transects separated by .5 m. The time window was set to 75 nanoseconds (ns) resulting in a maximum depth penetration of 3.07 m below surface.

ERT data was collected with the Advanced Geosciences, Inc. 56 probe SuperSting R8 IP eight-channel memory earthen resistivity and IP meter (Figure 5). Resistivity data was collected in both Dipole-Dipole and Inverse Schlumberger arrays. The Inverse Schlumberger array puts the current electrode pair inside the potential electrode pair, opposite of the traditional Schlumberger array, while the Dipole-Dipole configuration does not place the potential electrodes inside the current electrode pair (Hubbard 2009). Both the Dipole-Dipole and Inverse Schlumberger electrode configurations are useful in detecting lateral variations in the subsurface, but the Inverse Schlumberger is more sensitive in detecting vertical changes. The Dipole-Dipole array uses 8 channels during surveys, reducing the amount of survey time required to collect data in comparison to the Inverse Schlumberger, which uses only 4 channels.

The 56 probes were separated by an electrode spacing of 50 cm. Data were collected in four roll-along surveys (generated by moving sections of probes along the profile to create longer pseudosections). Because the field measurements are an indication of apparent ground resistivity values, inversion software is needed in order to convert these values in to a 2D resistivity model for analysis and interpretation (Loke 2010). Thus, field data were transferred from the SuperSting meter to a personal computer where it was processed using Advanced Geosciences, Inc. EarthImager 2D software package using the smooth model inversion method.

Down-hole data were collected with the Bartington MS2H down-hole sensor attached to a set of hollow aluminum extensions connected via coaxial cable to the Bartington MS2 display unit (Figure 6). The display unit connected to a laptop with a serial port for data collection. Readings were obtained every 2 cm at depths ranging from 10 cmbs to 300 cmbs. The system was set to measure volume susceptibility at a resolution of 1×10^{-5} SI units (Dalan 2006:170). Data were visualized using scatter plot line charts generated from Microsoft Excel, in addition to multi-core profile visualizations created in Golden Software's Voxler.



Figure 4. GPR data being collected atop Mound B with the GSSI SIR-3000 and 270 MHz antenna. Alex Craib and Sara Wyatt taking positional notes. Photograph by Vin Steponaitis.



Figure 5. ERT data collection with AGI 56 probe SuperSting R8 IP eight-channel memory earthen resistivity meter in process. Photograph by Megan Kassabaum.



Figure 6. Down-hole data collection underway with the Bartington Instruments, Inc. MS2H sensor, MS2 meter, and field laptop. Photograph by Vin Steponaitis.

SURVEY RESULTS

Geophysical results of the gradiometer and GPR surveys of the summit of Mound B at Feltus identified multiple anomalies that have angular patterns. ERT data collected over Mound B show a common horizontal linear low-resistivity anomaly inside the mound. Down-hole investigations on Mounds A and B revealed enhanced magnetic susceptibility at depths where internal mound variations were encountered in both excavation and hydraulic coring profiles. These anomalies are interpreted as the possible material remains of events associated with mound construction based on their size, shape, and enhancement. Additionally, curvilinear and amorphous anomalies located during the GPR surveys of Mound B can be attributed to burials encountered during excavations. Finally, down-hole data collected on Mound C by UNC-CH field school students Alex Craib and Sara Wyatt was converted into a color-scale profile and will be discussed here briefly.

MAGNETIC GRADIENT

A map of the gradiometer data atop Mound B at Feltus depicts a large angular high-susceptibility anomaly that is oriented in a rough u-shape (Figure 6). A few magnetic dipoles oriented north-south on top of Mound B indicate ferrous metal situated horizontally in the ground (Figure 7). A faint angular pattern extending across the survey is present as well. Two magnetic highs identified from the gradiometer survey were confirmed as burials during subsequent excavations (Figure 8).

GROUND-PENTRATING RADAR

The GPR survey of Mound B included the use of both a 400 and 270 shielded antennas. The results of the 400 MHz data indicate that multiple high amplitude reflection anomalies are present within the upper 80-90 cm of mound fill (Figure 9). Amplitude slice maps of 400 MHz GPR data from 21 to 36 cm below the top of Mound A exhibit a general rectangular pattern of anomalies on the summit (Figure 10). A smaller square anomaly is present in slice data between 31 and 67 cm below the surface (Figure 11).

Results of the 270 MHz GPR survey on Mound B indicate high amplitude reflection anomalies over 1.7 m into the mound fill (Figure 12). Some correlation is also observable between the rectangular anomaly in the shallow slices of the 400 MHz data and the 270 MHz data (Figure 13).

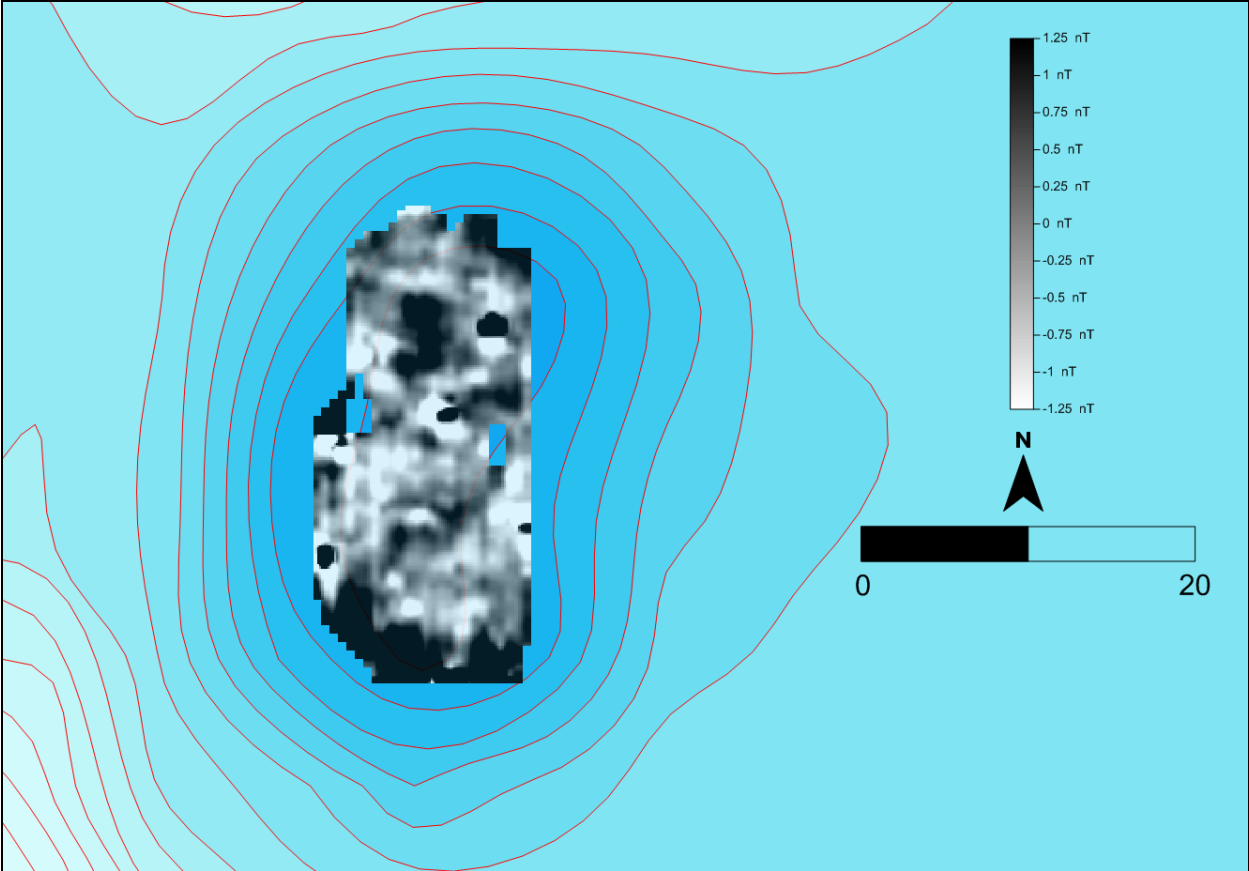


Figure 6. Magnetic gradient results from the summit of Mound B at Feltus. Contours exhibit 1.5 meter elevation changes. Scale bar is in meters. Map by the authors.

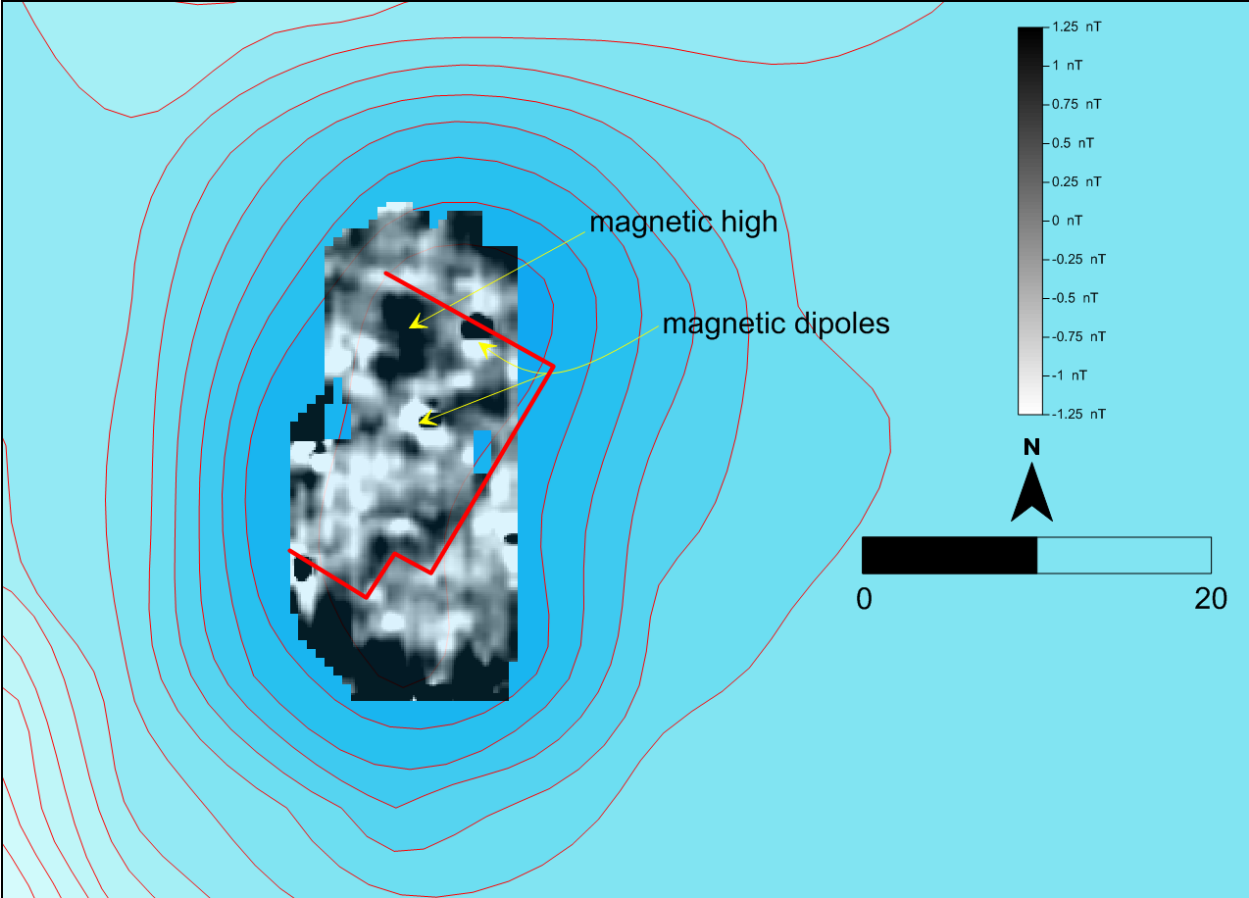


Figure 7. Magnetic gradient anomalies from Mound B at Feltus. Faint magnetic outline delineated with red line. Contours exhibit 1.5 meter elevation changes. Scale bar is in meters. Map by the authors.

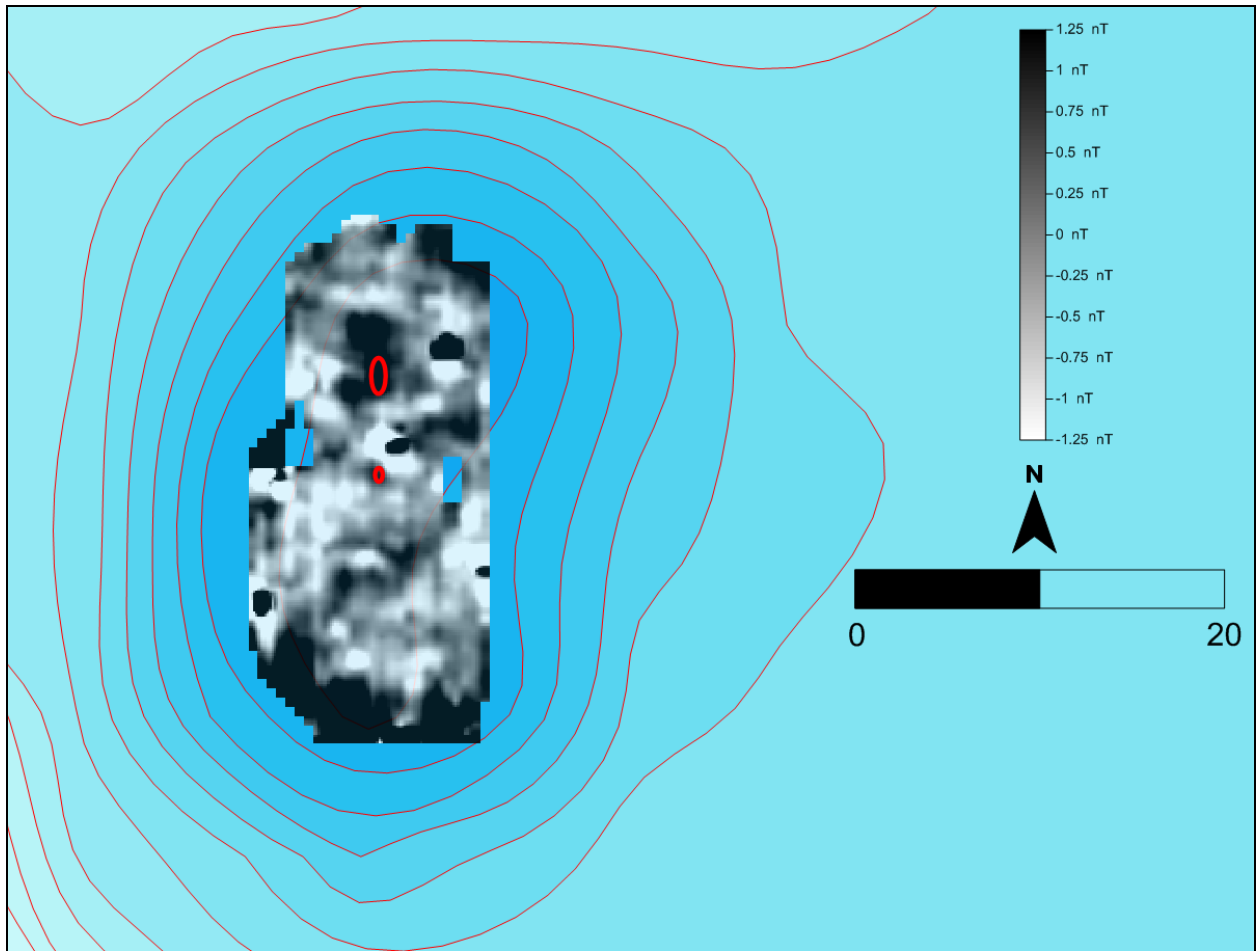


Figure 8. Location of burials in red on top of gradiometer data. Contours exhibit 1.5 meter elevation changes. Scale bar is in meters. Map by the authors.

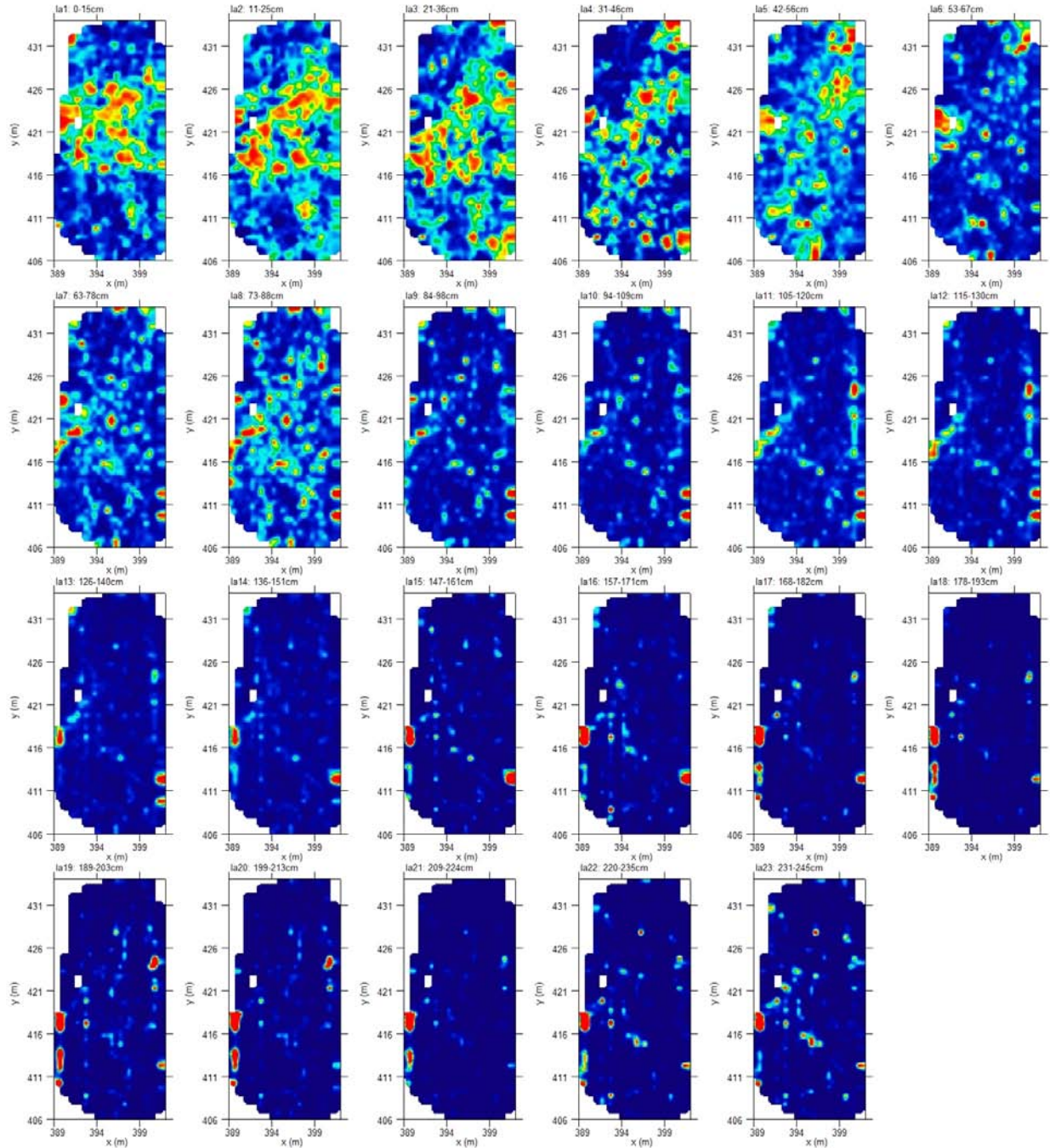


Figure 9. Amplitude slice maps of 400 MHz GPR data from the summit of Mound B. Map by the authors.

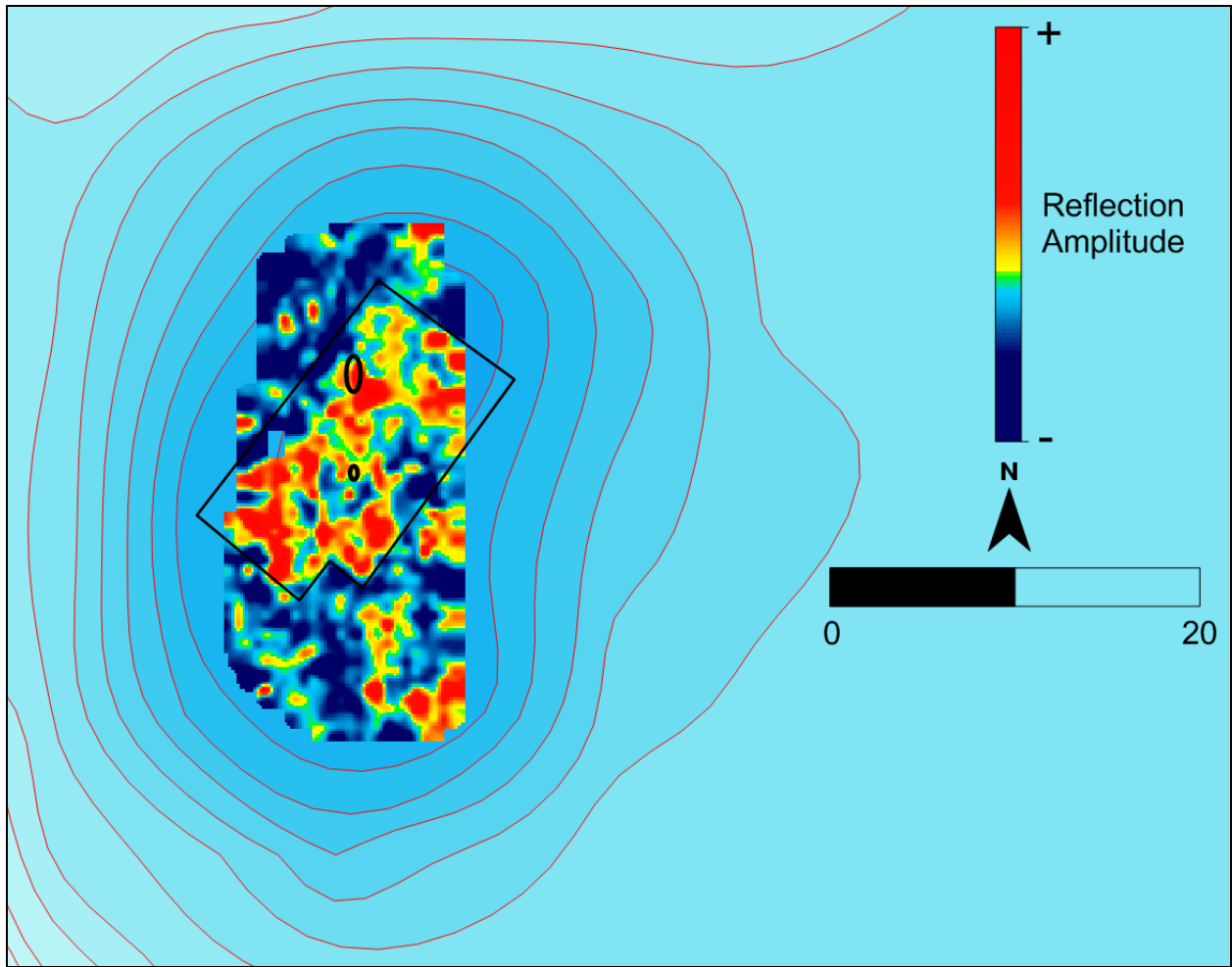


Figure 10. Amplitude slice map of 400 MHz GPR data from 21 to 36 cmbs. Angular anomaly and burials outlined in black. Contours exhibit 1.5 meter elevation changes. Scale bar is in meters. Map by the authors.

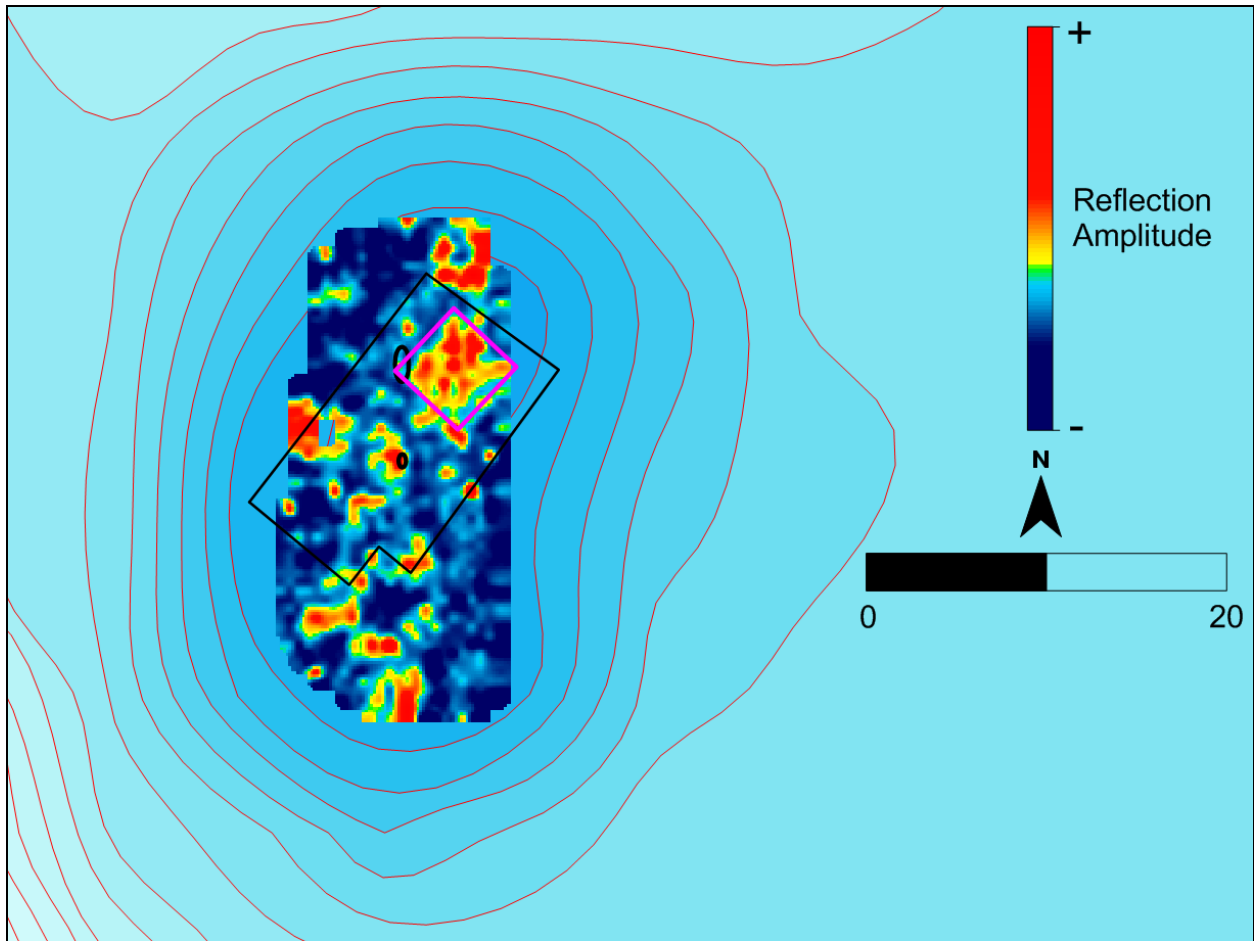


Figure 11. Amplitude slice map of 400 MHz GPR data from 42 to 56 cmbs. Angular anomaly and burials outlined in black. Square anomaly outlined in magenta. Contours exhibit 1.5 meter elevation changes. Scale bar is in meters. Map by the authors.

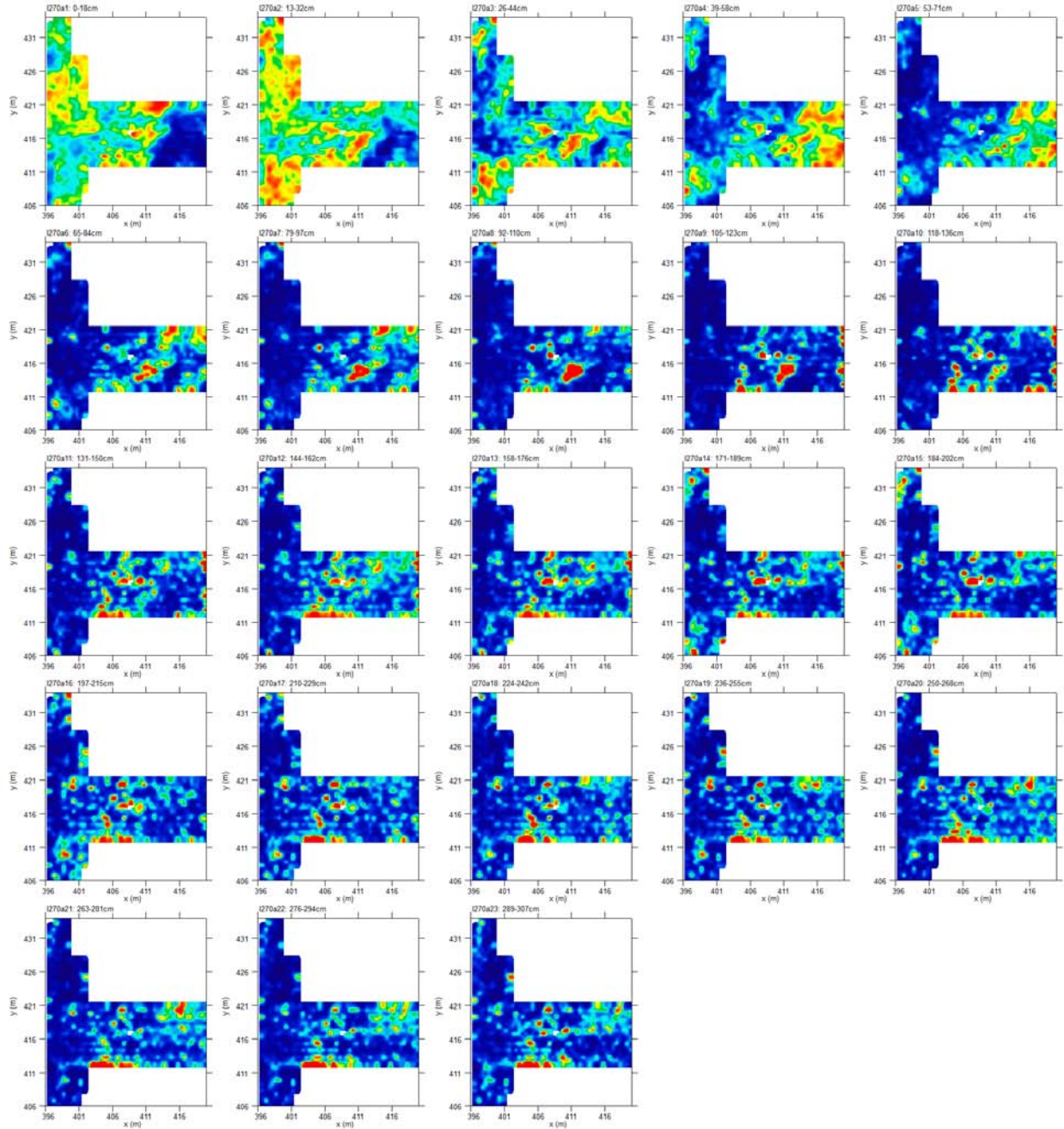


Figure 12. Amplitude slice maps of 270 MHz GPR data from the summit of Mound B. Map by the authors.

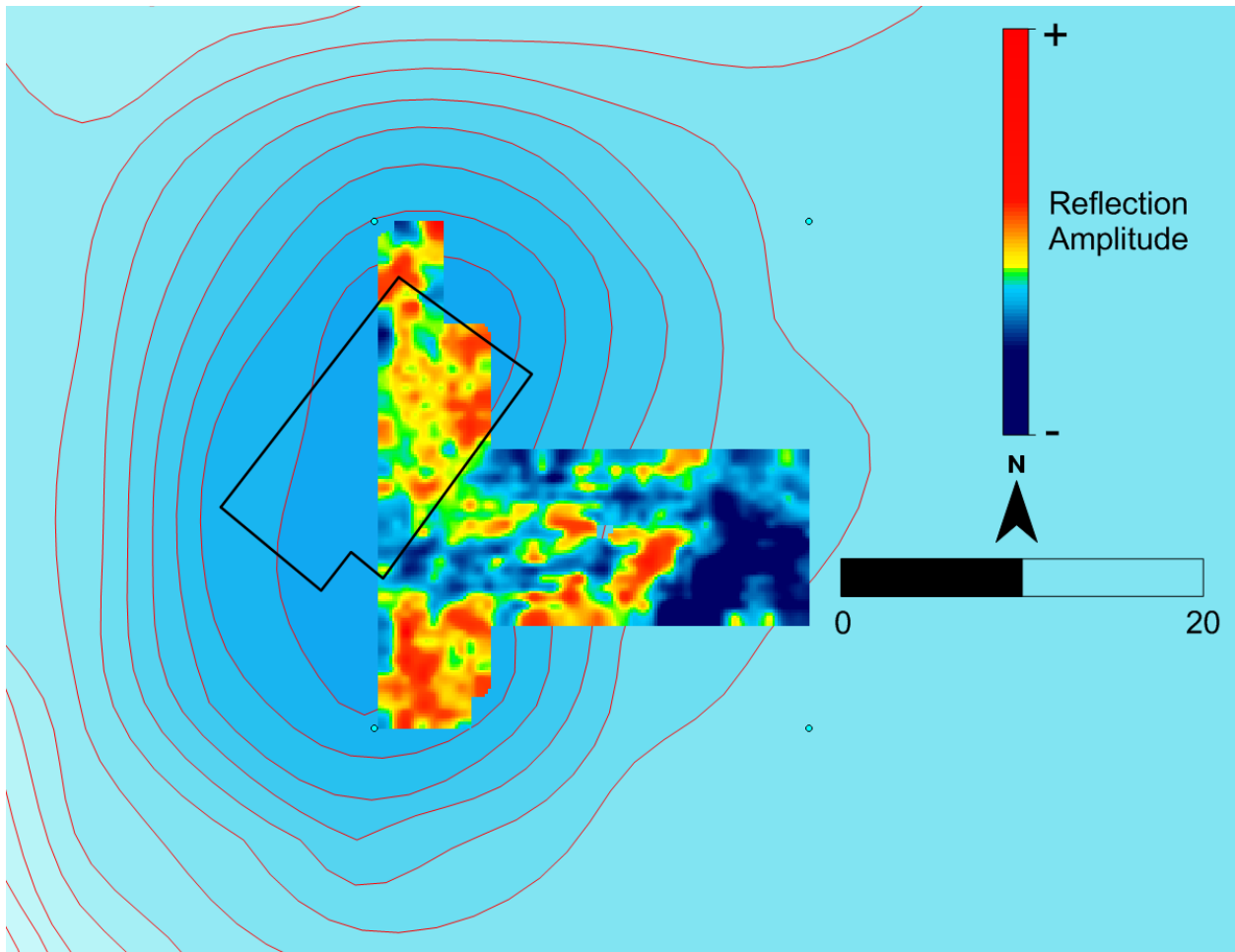


Figure 13. Amplitude slice map of 270 MHz GPR data from 13 to 32 cmbs. Angular anomaly from 400 MHz data outlined in black. Contours exhibit 1.5 meter elevation changes. Scale bar is in meters. Map by the authors.

ELECTRICAL RESISTIVITY TOMOGRAPHY

ERT data were collected over four profiles on Mound B to assess internal variation (Figure 14). Profile 1 was collected in both a dipole-dipole array and an inverse Schlumberger array to determine which array would best depict internal mound variation. The dipole-dipole array recorded many more data points and took much more time to run. Results of the dipole-dipole array show a lateral band of moderate resistivity near the surface of Mound B, and another below it exhibiting low resistivity (Figure 15). High resistivity locales near the base of the profile are also present in this pseudosection. The inverse Schlumberger array showed similar lateral trends in the data and took much less time to run (Figure 16). Given the amount of time saved with the inverse Schlumberger array and the similarity in terms of results, the rest of the ERT data on Mound B were collected using the inverse Schlumberger array.

ERT data from Profile 2 exhibit remarkable similarity to Profile 1 (Figure 17). Moderate to high resistivity extends across the near surface of the mound, while a lateral low resistivity anomaly stretches across the mound just below it. High resistivity anomalies are also present below the lateral low resistivity anomaly. Results of the ERT data from Profile 3 show what appears to be the remnants of the lateral low resistivity anomaly within the mound, but the lower pockets of high resistivity are not as well documented (Figure 18). This ERT profile was not as centrally located on the mound and therefore may be showing a boundary of the low resistivity anomaly. The north-south oriented Profile 4 demarcated the internal lateral low resistivity anomaly very well (Figure 19). Below it, zones of moderate to high resistivity undulated within the mound.

DOWN-HOLE MAGNETIC SUSCEPTIBILITY

Series of consecutive down-hole cores were placed on the east and southern flanks of Mound A and on the eastern flank of Mound B (Figure 20). Additionally, a series of cores were placed over Mound C, extending through the ditch in front of the mound. These cores were removed and examined by UNC-CH field school students Alex Craib and Sara Wyatt as part of an independent study.

The first series of down-hole cores examined were on the eastern flank of Mound A. These 16 cores were separated by a meter and were situated parallel to, and 20 cm north from the northern profile of a trench excavated by UNC-CH archaeologists in 2006 (Vin Steponaitis and Megan Kassabaum, personal communication 2012). The down-hole profile exhibits mostly moderate susceptibility in the upper portions of the mound (Figure 21). However, a linear area of high susceptibility is present across the mound profile around an elevation of 73.4 m. Additionally, a basin-shaped anomaly of high susceptibility is noticeable near the 532 easting core. A lateral band of high susceptibility is present just below this anomaly. The down-hole data from the southern flank of Mound A show similar enhancement of susceptibility within the mound (Figure 22). A linear area of high susceptibility around 73.2 m in elevation corresponds with the linear enhancement on the eastern flank. Further, the high susceptibility near the toe of the Mound A slope corresponds with the level of high susceptibility on the eastern flank, both running roughly level at approximately 69.2 m in elevation.

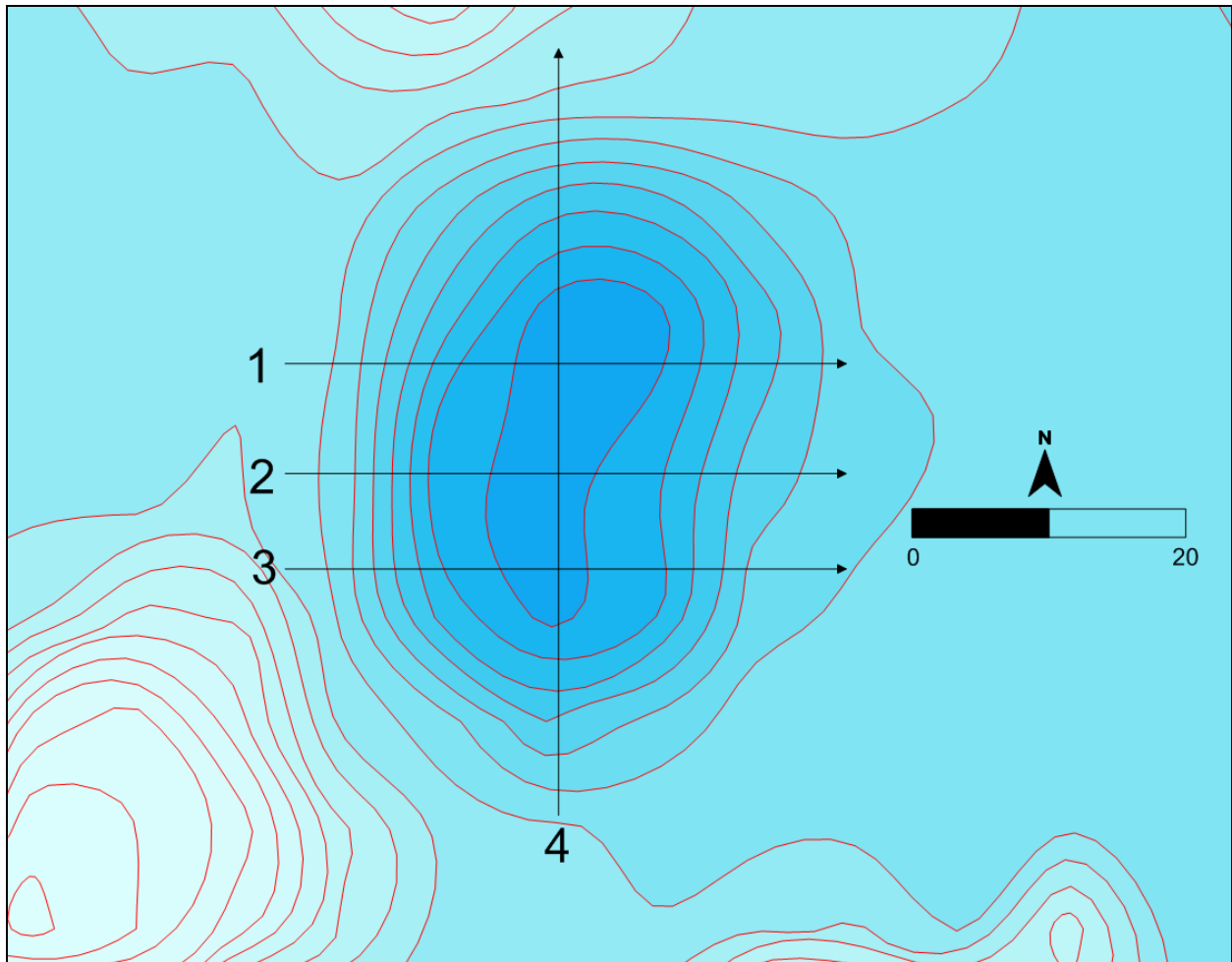


Figure 14. Location of ERT profiles on Mound B at Feltus. Contours exhibit 1.5 meter elevation changes. Scale bar is in meters. Map by the authors.

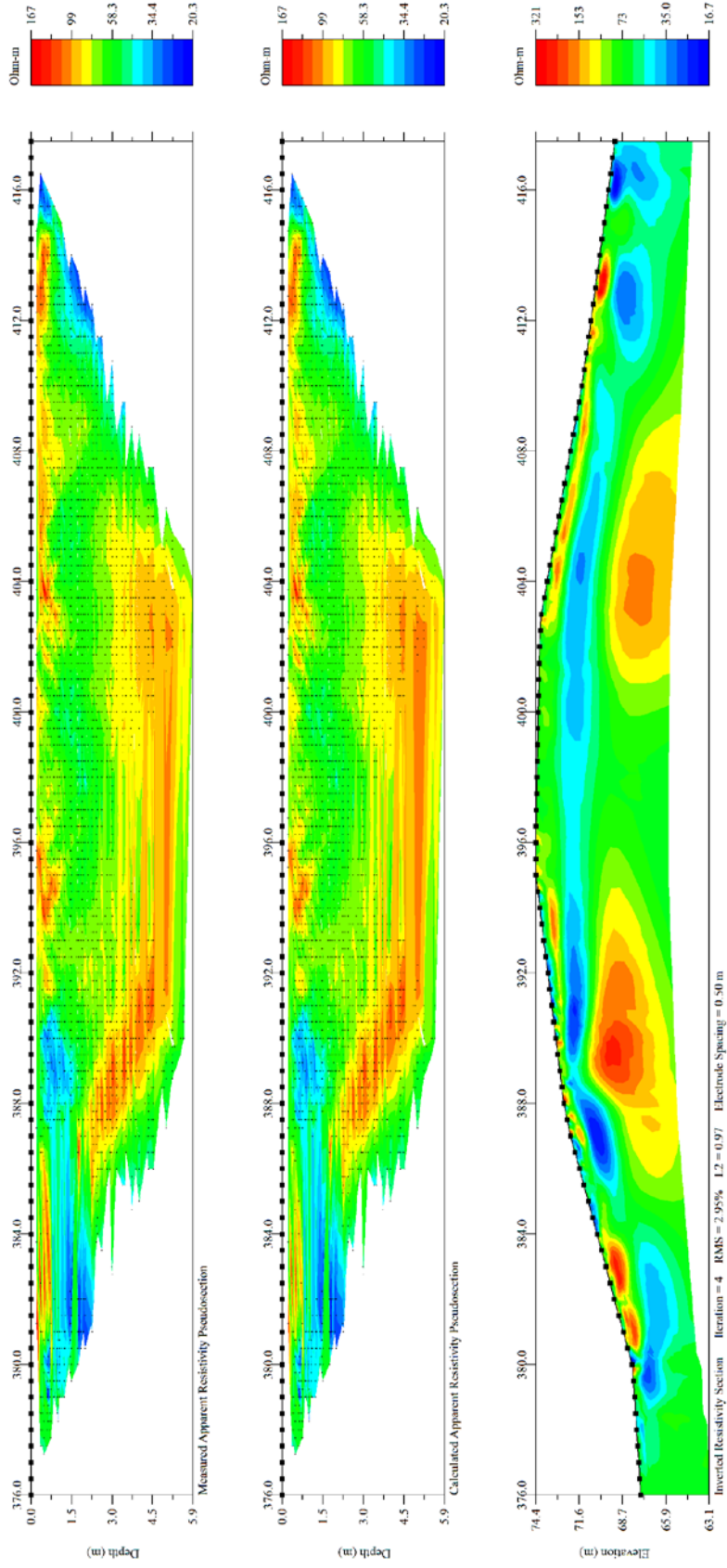


Figure 15. Pseudosection of ERT profile 1 collected with dipole-dipole array. Map by the authors.

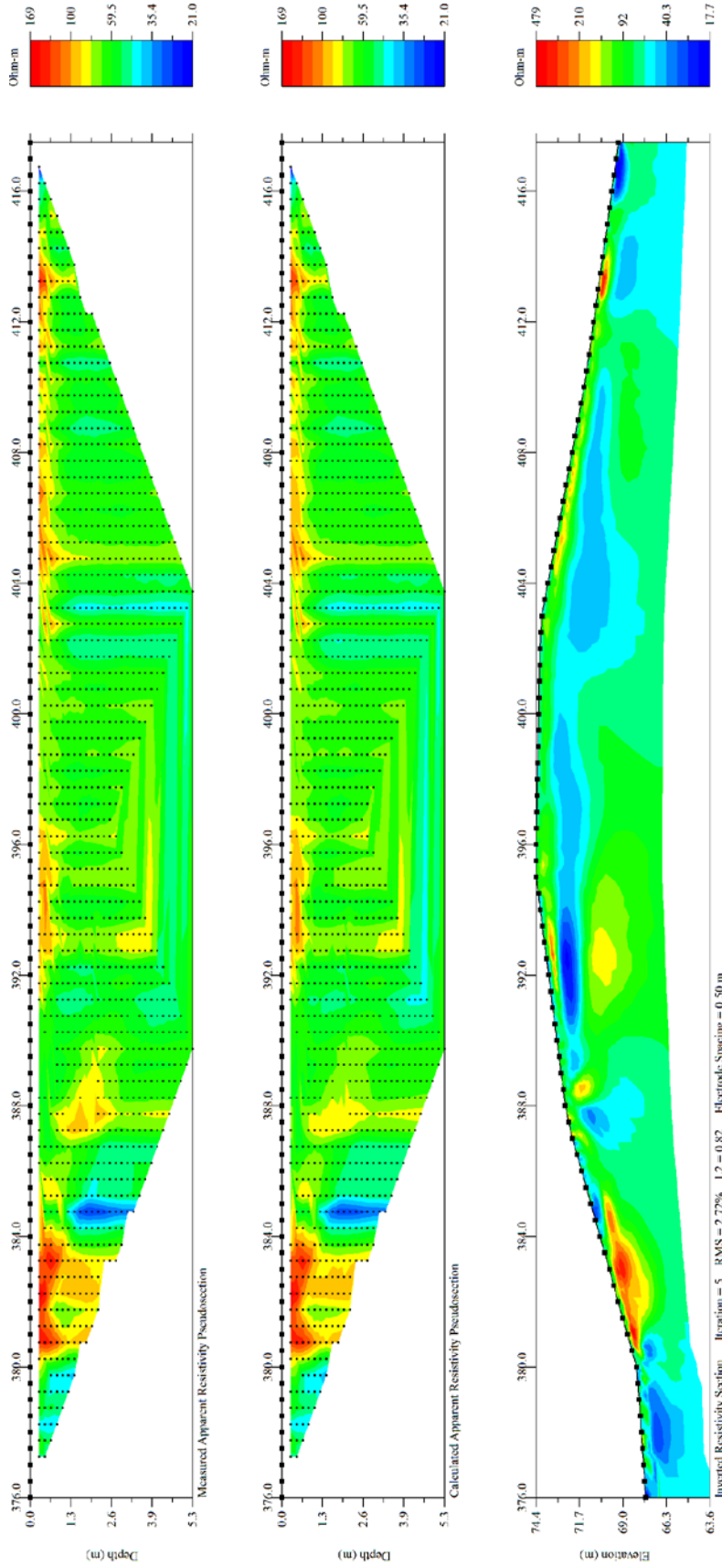


Figure 16. Pseudosection of ERT profile 1 collected with inverse schlumberger array. Map by the author.

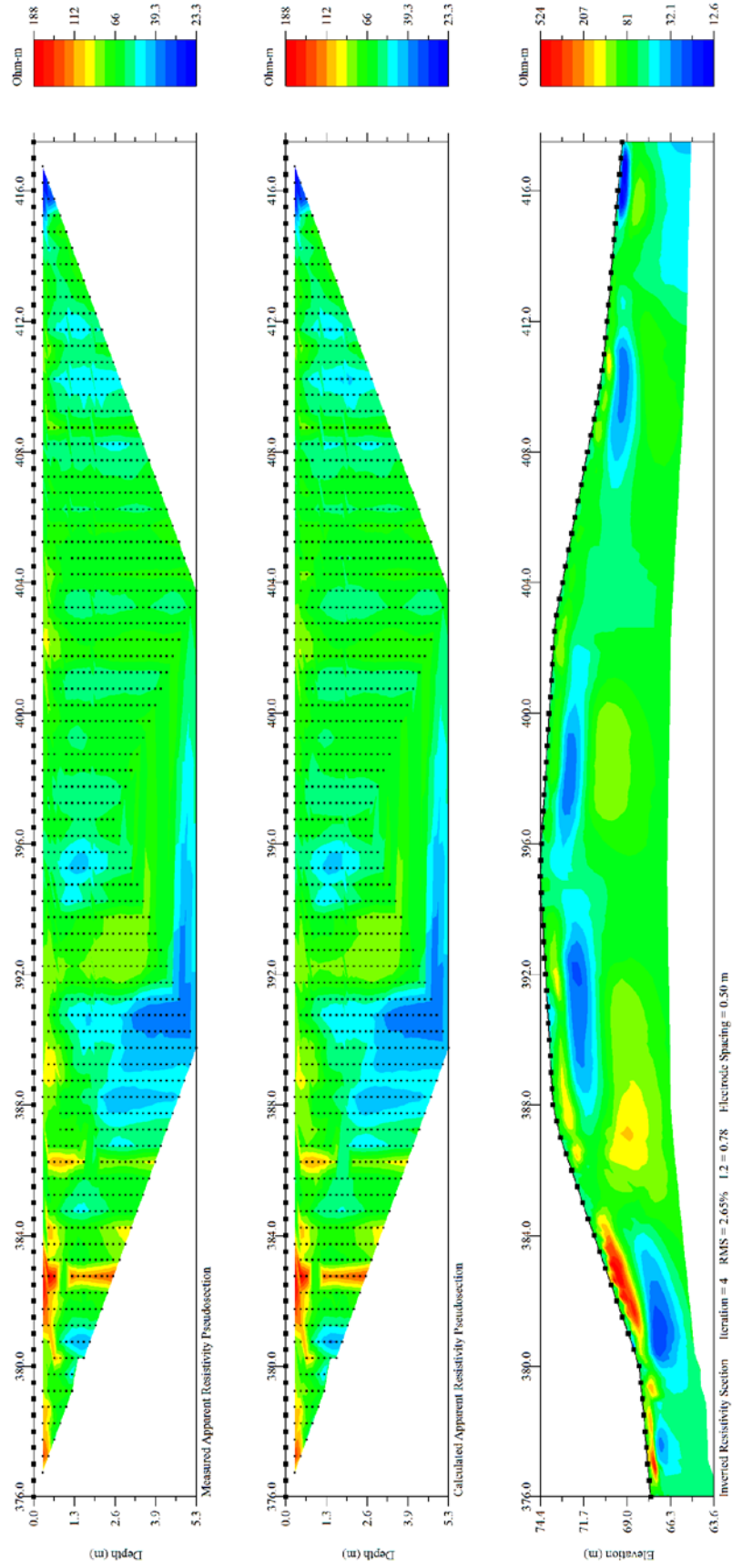


Figure 17. Pseudosection of ERT profile 2 collected with inverse schlumberger array. Map by the authors.

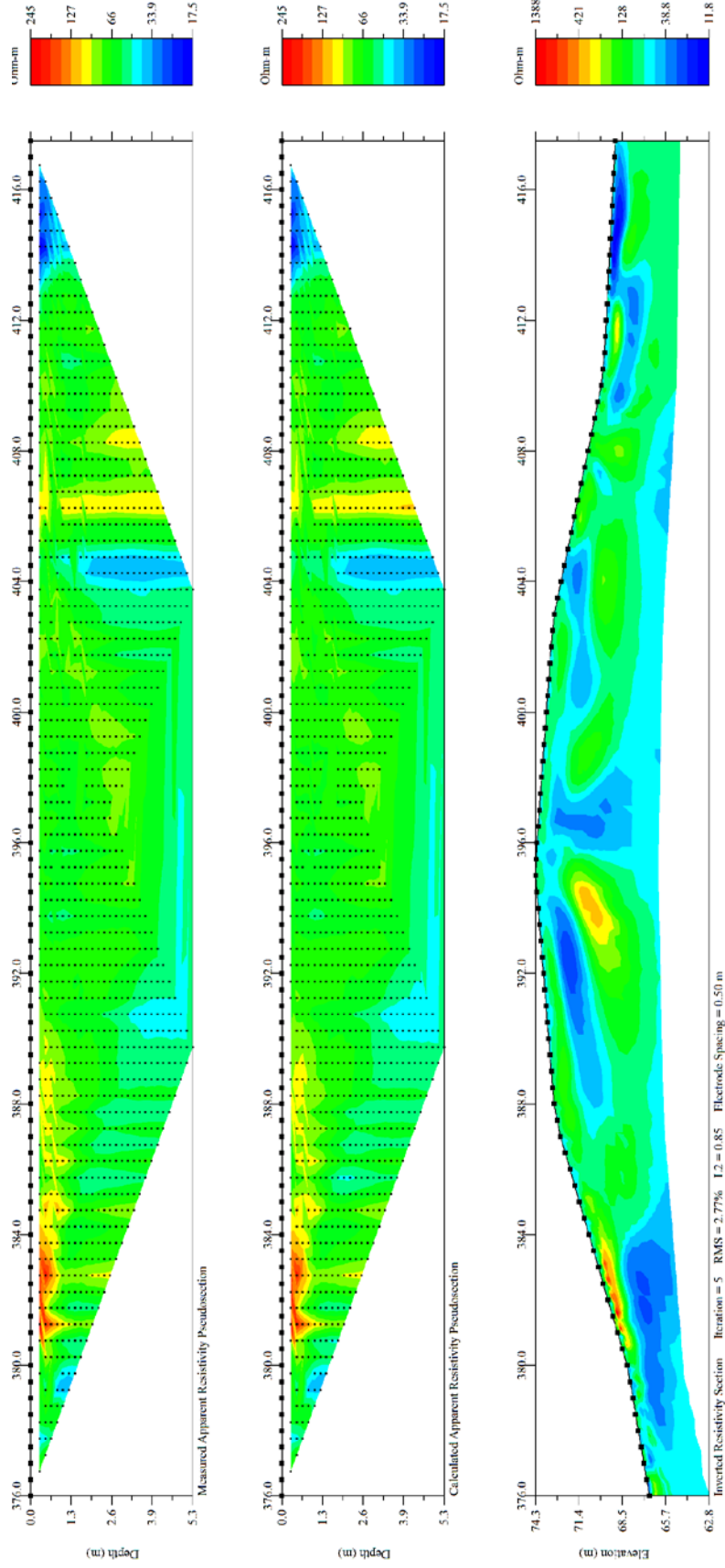


Figure 18. Pseudosection of ERT profile 3 collected with inverse schlumberger array. Map by the authors.

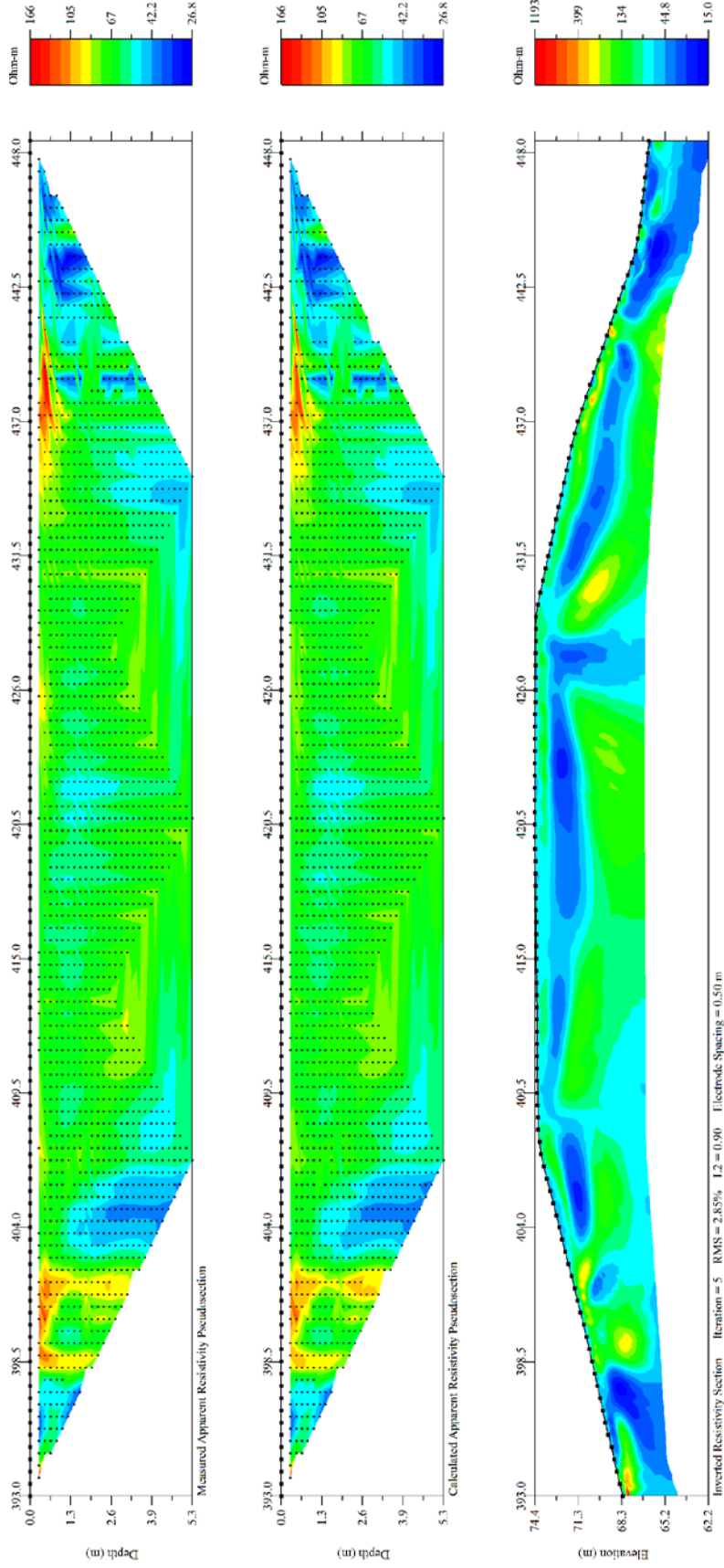


Figure 19. Pseudosection of ERT profile 4 collected with inverse schlumberger array. Map by the authors.

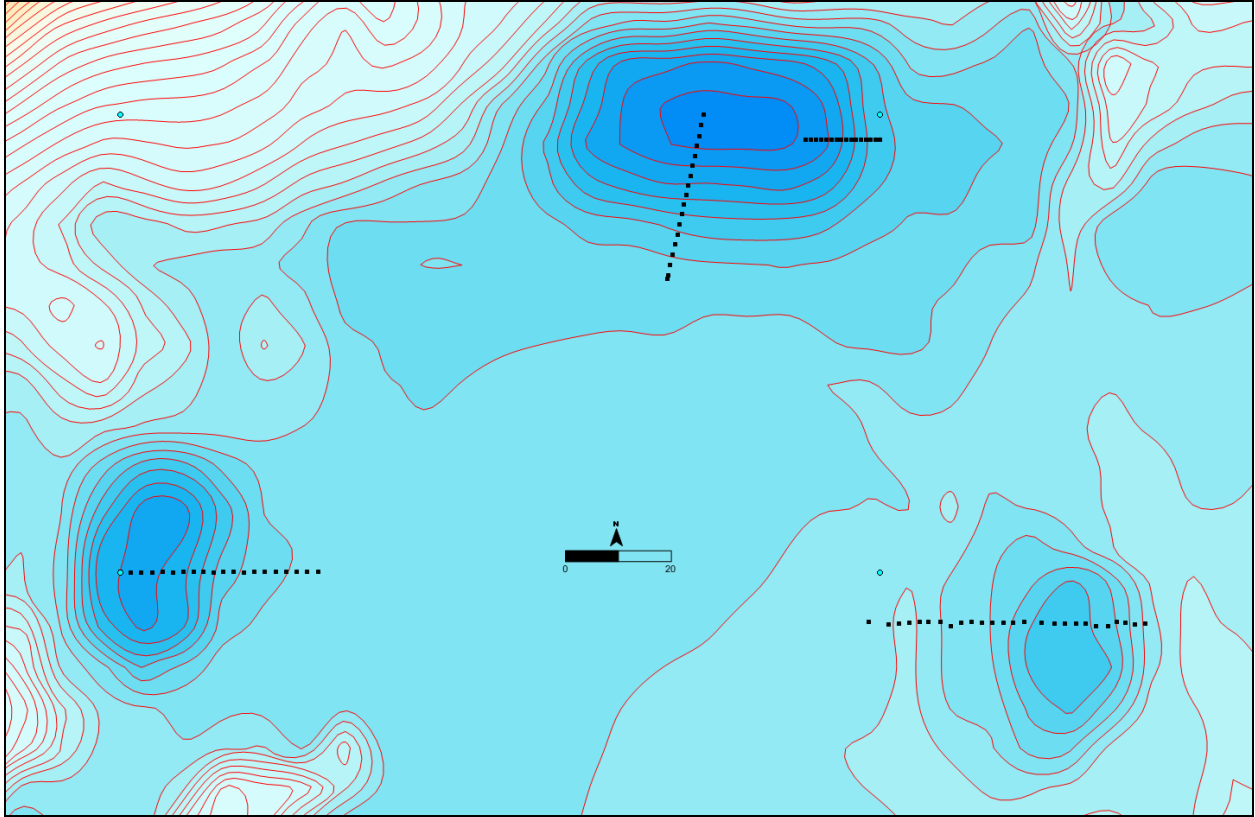


Figure 20. Location of down-hole cores at Feltus. Contours exhibit 1.5 meter elevation changes. Scale bar is in meters. Map by the authors.

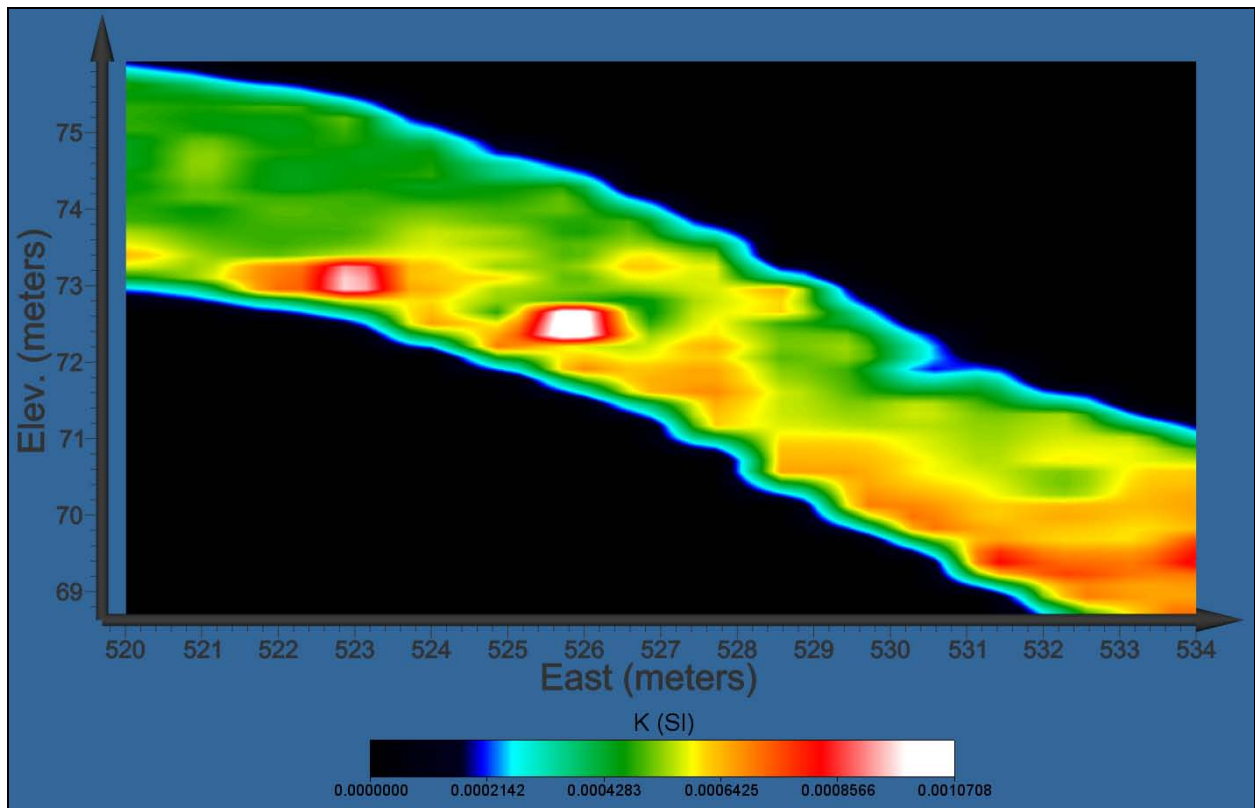


Figure 21. Down-hole data from Eastern flank of Mound A. Map by the authors.

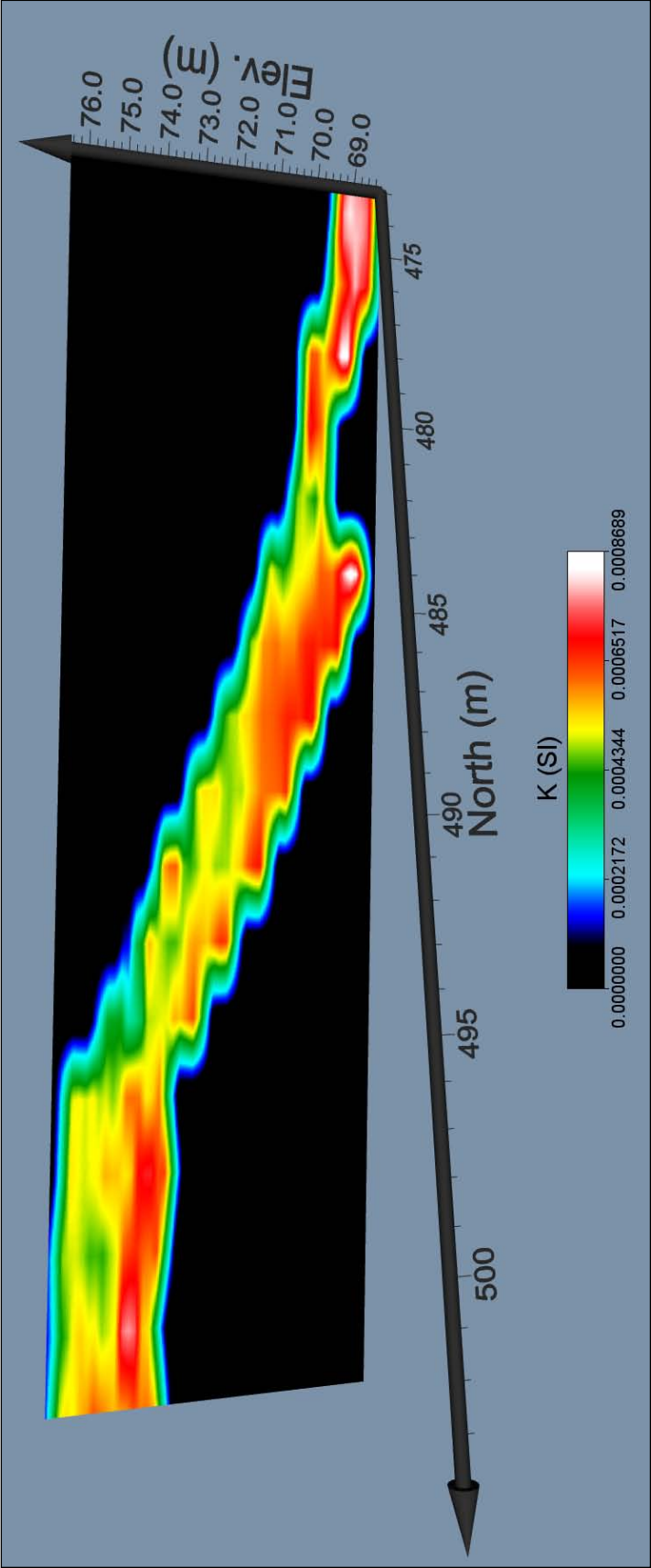


Figure 22. Down-hole data from Southern flank of Mound A. Map by the authors.

In addition to down-hole investigations on Mound A, one series of cores was placed, oriented east-west, on the top and eastern flank of Mound B. This line of cores was situated to coincide with the ERT pseudosection profile 2. The results from these cores indicate a linear area of high susceptibility beneath the low lying apron that extends east of Mound B (Figure 23). High susceptibility values are also clustered at the easternmost two cores. A lateral anomaly of high susceptibility is present inside the mound at an elevation of 72.5 m.

Results of data collected on Mound C by UNC-CH field school students Alex Craib and Sara Wyatt show multiple internal mound anomalies (Figure 24). One lateral anomaly of high susceptibility extends across the interior portions of the mound at an elevation of 69.5 m. The apron extending between the main mound and the ditch exhibits a large lateral area of high susceptibility at an elevation of 67.2 m as well. High susceptibility values in the ditch are isolated to two cores that could penetrate deep enough to get a suitable amount of data. These cores exhibit moderate to high values in the ditch.

COMPARISON OF DATASETS AND DISCUSSION

The data collected across these three mound contexts at Feltus provide a means by which to examine relationships between geophysical variation and excavation results. Each of the three mounds has excavation data corresponding to at least one portion of the geophysical investigations conducted there. The three mounds will be discussed here in relation to both geophysical results and stratigraphic information obtained from excavation and hydraulic coring.

MOUND A

The data from down-hole cores placed on Mound A can be compared with the stratigraphic data from an excavation trench on the eastern flank of the mound and 3-inch hydraulic cores removed from the top of the mound. The data from the magnetic susceptibility profile paralleling the eastern flank trench reveals numerous lateral trends in high susceptibility (Figure 21). Previous excavations and coring have identified floors in this mound at approximately 73.5 m and 71.7 m in elevation, as well as a submound midden at 69.55 m (Vin Steponaitis, personal communication 2012). The floor at 73.5 m can be seen in the eastern and southern flank susceptibility profiles and these floors were visible in cores removed in these areas. The submound midden is also present in both profiles and was easily seen in cores that penetrated this zone. However, another lateral anomaly of high susceptibility is observable in the southern flank profile on Mound A at 74.5 m. The cores in this anomaly note a red ashy layer with burned daub. Thus, this anomaly may represent a feature extending across this portion of Mound A.

Aside from floors in Mound A, the down-hole profile on the eastern flank exhibited variations that correspond with a feature encountered in the trench excavations. A basin-shaped moderate susceptibility anomaly that is underlain by high susceptibility is located between the easting of 529 and 534 (Figure 21). This anomaly matches the location of a “bathtub shaped” pit feature encountered in the wall of this trench, just above the submound midden (Vin Steponaitis, personal communication 2012).

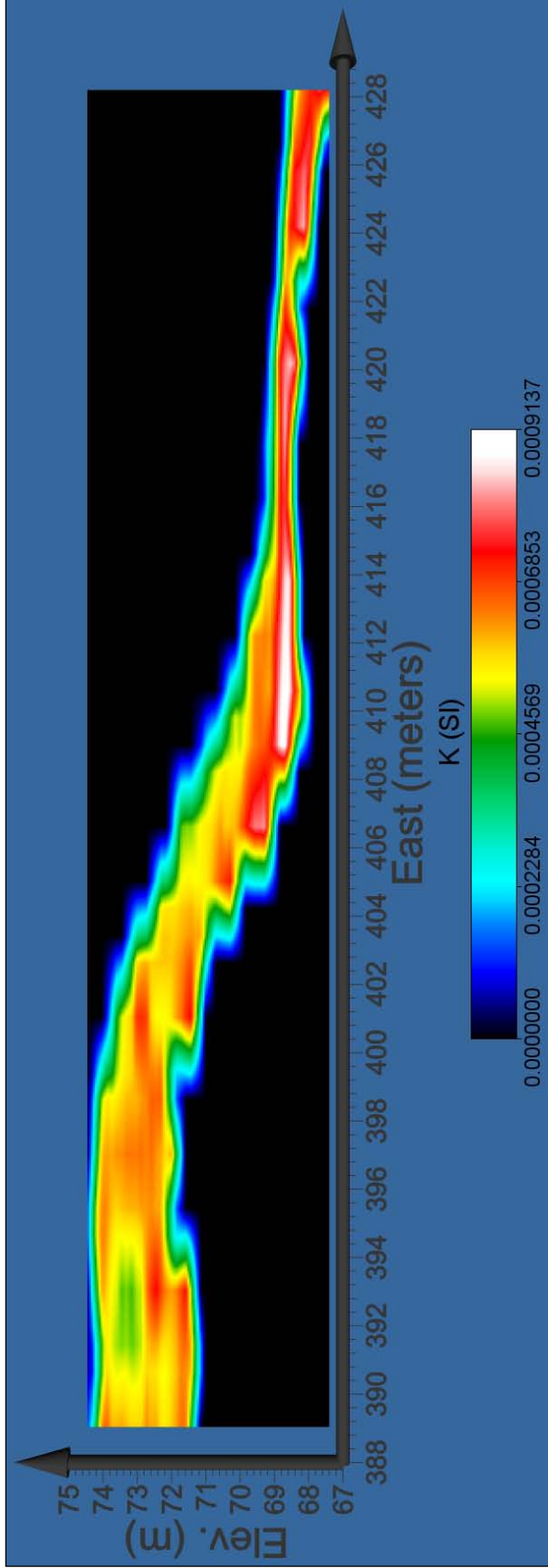


Figure 23. Down-hole data from Eastern flank of Mound B. Map by the authors.

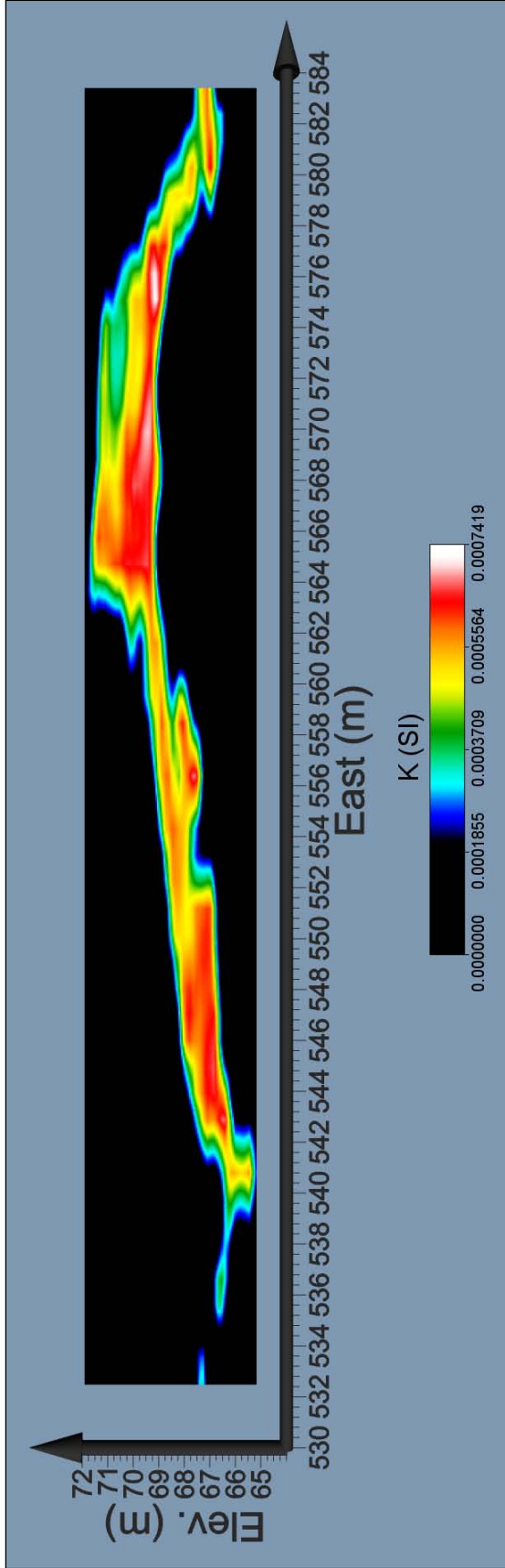


Figure 24. Down-hole data from Mound C. Map by the authors from data collected by Craib and Wyatt (2012).

MOUND B

Datasets collected on Mound B included gradiometer, ERT, GPR, and down-hole. These four datasets can be compared to stratigraphy documented from excavations and hydraulic coring on this mound. Excavation trenches are situated east-west on the western flank of the mound and north-south across the mound summit. Magnetic gradient and 400 MHz GPR anomalies corresponded to burials that were encountered during excavation of the north-south trench on the summit. Similar anomalies are present on the northern half of the summit, suggesting that other burials could be present near this area.

ERT data from this mound depicts a linear low resistivity anomaly running across the mound at approximately 72.25 m in elevation (Figures 16 and 17). Given that ERT profile 3 and the down-hole profile are situated on the same northing coordinate, direct comparison can be made with the data. Additionally, the 270 MHz GPR data collected in this area was topographically corrected to adjust for antenna tilt, making a third directly comparable dataset to the ERT and down-hole profiles. The ERT profile from this area shows the linear anomaly under the surface of the mound; however another low resistivity anomaly is present around the 409 to 410 easting at an elevation of 70 m (Figure 25). When the down-hole data are overlaid onto this profile, correlations with linear anomalies of high susceptibility and the linear anomalies of low resistivity become apparent (Figure 26). A linear anomaly of very high susceptibility extends east from beneath the major slope of Mound B. When the topographically corrected radar profile is superimposed on the ERT data from Profile 3, few correlations are visible. However, one area containing high amplitude radar reflections corresponds to the area of low resistivity on the eastern slope of Mound B and in an area extending eastward where high susceptibility was observed (Figure 27).

A common feature encountered in excavations on this mound is prepared clay floors. A submound midden underlies Mound B as well. Floors 5 and 4 are situated at an approximate elevation of 72.75 m and 71.80 m respectively. The submound midden is positioned at an elevation of 68.80 m (Vin Steponaitis, personal communication 2012). Comparing the position of these internal mound features allows a more accurate depiction of the geophysical results from Mound B. The upper linear high in the down-hole data and the upper low resistivity anomaly corresponds well with Floor 5. Floor 4 corresponds with the lower portion of the linear low resistivity anomaly. High susceptibility caps the ends of this floor, making the edges visible but its extent through the center of the mound cannot be established due to lack of data. The submound midden is visible in the down-hole data. The low resistivity anomaly near the eastern base of Mound B has correlates of high susceptibility in the down-hole data and high reflection amplitude in the GPR data. Given the correlations of the floors with the multiple geophysical results, it is possible that the lower anomalies may correlate to a construction stage that underlies the primary mound. This may be a low, wide platform on top of which Mound B was constructed.

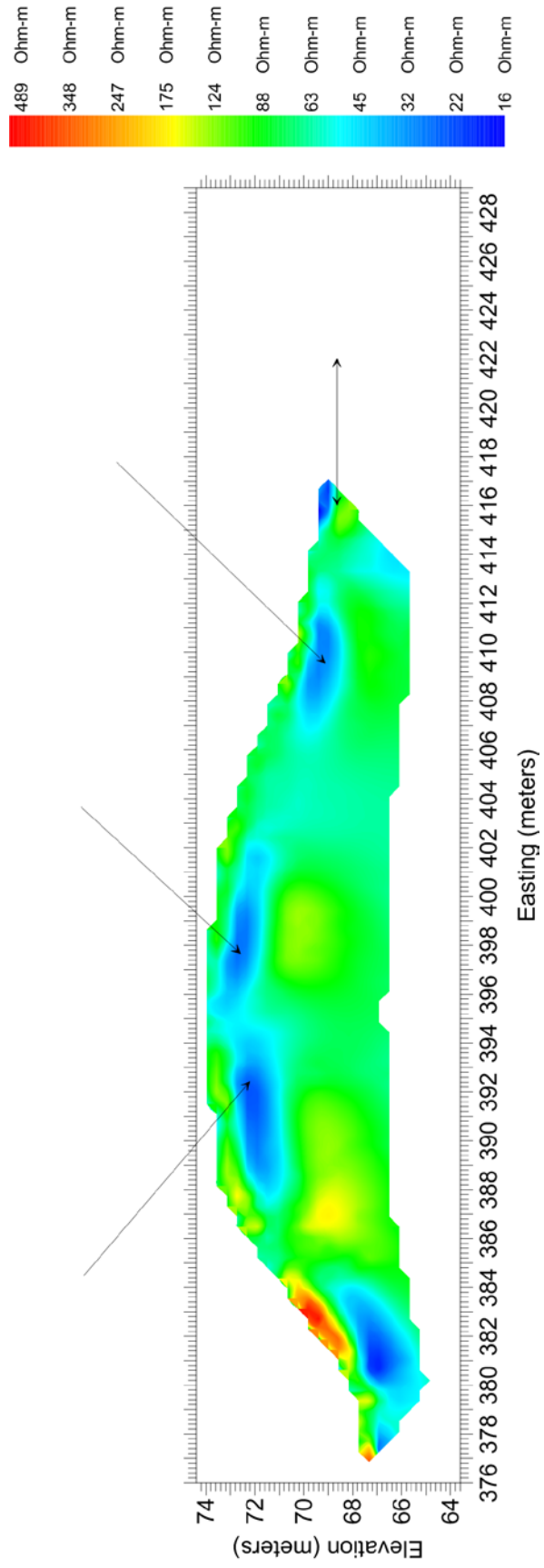


Figure 25. ERT Profile 3 from Mound B. Map by the authors.

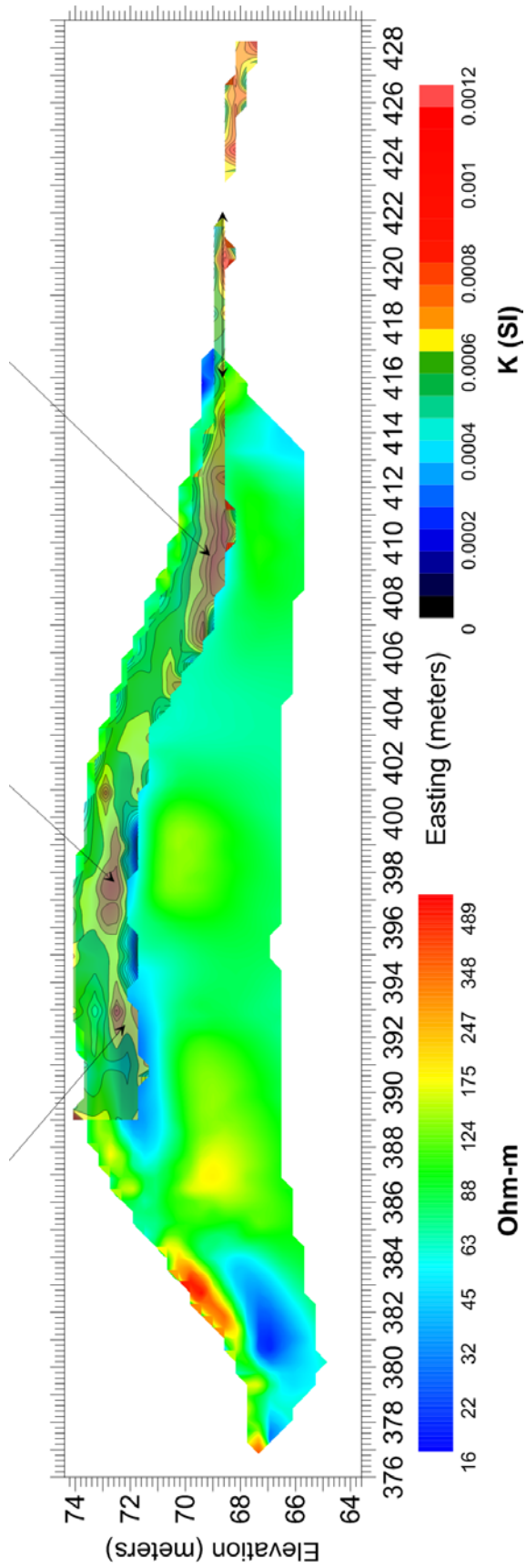


Figure 26. Down-hole data from Mound B set at 60 percent opacity and overlaid onto ERT Profile 3. Map by the authors.

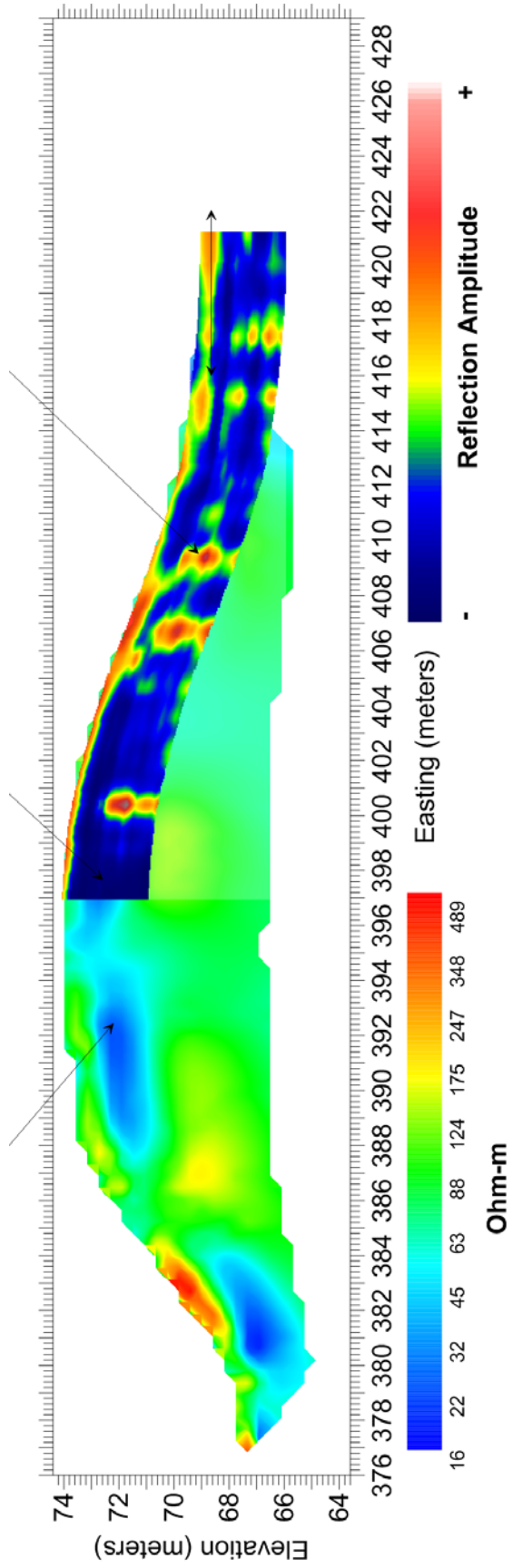


Figure 267 GPR data from Mound B overlaid onto ERT Profile 3. Map by the authors.

MOUND C

The down-hole results over Mound C show linear anomalies of high susceptibility inside the mound and to the west between the mound and the ditch (Figure 24). Visualization of this data show that a previous “low-tech” depiction of the data created by Craib and Wyatt (2012) mapped significant variations within the mound. Their interpretations of the data outlined the mapping of the original ground surface at 67.4-67.2 m in elevation, the top of the first construction stage around 68.43 m, the second stage at 68.67, and the third stage at 69.55 m (Craib and Wyatt 2012:5-6). These stages match anomalies depicted in the visualization created with Voxler (Figure 24). However, the high susceptibility values in the few cores in the ditch west of Mound C leave the possibility that it was excavated prehistorically.

CONCLUSIONS

The multi-instrument geophysical investigations of Mounds A, B, and C at Feltus Mounds in Jefferson County, Mississippi succeeded in mapping the extent of multiple construction episodes and archaeological features internal to the mounds. Techniques used in these investigations included a gradiometer, GPR, ERT, and down-hole magnetic susceptibility sensor. When compared to known stratigraphic relationships observed in excavation and hydraulic coring, the geophysical data can be used to assess how extensive these features are within the mound. In Mound A multiple floors were mapped with the down-hole sensor. Further, the submound midden was recorded in the data from Mound A. The upper floor that was possibly mapped on the summit in the southern down-hole profile on Mound A may be a new floor not yet encountered in excavation.

Investigations on Mound B suggest more burials may be present in the northern half of Mound B’s summit. Additionally, two floors and the submound midden were mapped with the ERT, GPR, and down-hole. The data indicate that these floors may cover the entire extent of the mound at a given time. Other correlations between these datasets support an interpretation that a low-wide platform was first erected on the midden prior to the majority of Mound B constructed on the western side of this platform.

The down-hole profile over Mound C also indicates that the majority of Mound C may have been constructed on a low-wide platform. The first construction stage is not very thick and extends laterally across the entire base of the mound where data is present. Other lateral susceptibility anomalies relate to known floors documented in coring and excavation. The main question that Mound C investigations leave is whether the ditch was excavated prehistorically? Other susceptibility studies on ditched earthworks indicate that they typically refill with highly magnetic topsoil (Burks and Cook 2011, Henry 2011). High susceptibility values in the few cores excavated through the ditch west of Mound C at Feltus suggest that a highly magnetic matrix has refilled the ditch, but it does not indicate whether the ditch was excavated prehistorically. The regularity of the ditched feature is certainly suggestive of such a circumstance.

BIBLIOGRAPHY

Aitken, M.J.

1961 *Physics and Archaeology*. Interscience Publishers, New York.

Aspinall, A., C. Gaffney, and A. Schmidt

2008 *Magnetometry for Archaeologists*. Alta Mira Press, New York.

Astin, T., H. Eckardt, and S. Hay

2007 Resistivity Imaging Survey of the Roman Barrows at Bartlow, Cambridgeshire, UK.
Archaeological Prospection 14(1):24-37. DOI: 10.1002/arp.287

Bevan, B. W.

1975 A magnetic survey at Les Forges du Saint Maurice. *MASCA Newsletter* (Museum Applied Science Center for Archaeology) 11(2):1.

1998 *Geophysical Exploration for Archaeology: An Introduction to Geophysical Exploration*. Midwest Archaeological Center, Special Report No. 1. National Park Service, Lincoln, Nebraska.

Bevan, B. W., and J. Kenyon

1975 Ground-penetrating radar for historical archaeology. *MASCA Newsletter* (Museum Applied Science Center for Archaeology) 11(2):2-7.

Burks, J.A. and R. A. Cook

2011 Beyond Squier and Davis: Rediscovering Ohio's Earthworks Using Geophysical Remote Sensing. *American Antiquity* 76(4):667-689.

Clark, A.

1996 *Seeing Beneath the Soil, Prospecting Methods in Archaeology*. 2nd Ed. B. T. Batsford Ltd., London.

Conyers, L. B.

2004 *Ground-Penetrating Radar for Archaeology*. Alta Mira Press, New York.

Conyers, L. B. and D. Goodman

1997 *Ground-Penetrating Radar: An Introduction for Archaeologists*. Alta Mira Press, New York.

Conyers L. B. and J. Leckebusch

2010 Geophysical Archaeology Research Agendas for the Future: Some Ground-penetrating Radar Examples. *Archaeological Prospection* 17(2):117-123. DOI: 10.1002/arp.379.

- Craib, A. and S. Wyatt
 2012 *Down Hole Magnetic Susceptibility Survey Of Mound C at Feltus*. Unpublished paper submitted in partial fulfillment of an independent study associated with the 2012 University of North Carolina-Chapel Hill field school at Feltus Mounds.
- Dalin, R. A.
 2001 A Magnetic Susceptibility Logger for Archaeological Application. *Geoarchaeology* 16(3):263-273.
- 2006 Magnetic Susceptibility. In *Remote Sensing in Archaeology: An Explicitly North American Perspective*, edited by J. K. Johnson, pp. 161-203. The University of Alabama Press, Tuscaloosa.
- Gaffney, C., and J. Gater
 2003 *Revealing the Buried Past: Geophysics for Archaeologists*. Tempus Publishing Ltd, Stroud, Gloucestershire.
- Henry, E. R.
 2011 A Multi-Stage Geophysical Approach to Detecting and Interpreting Archaeological Features at the LeBus Circle, Bourbon County. KY. *Archaeological Prospection*. In Press. DOI: 10.1002/arp.418
- Hubbard, J. L.
 2009 *Use of Electrical Resistivity and Multichannel Analysis of Surface Wave Geophysical Tomography in Geotechnical Site Characterization of Dam*. Unpublished Thesis, The University of Texas at Arlington.
- Johnson, J. K., editor
 2006 *Remote Sensing in Archaeology: An Explicitly North American Perspective*. University of Alabama Press, Tuscaloosa.
- King, A., C. P. Walker, R. V. Sharp, F. K. Reilly, and D. P. McKinnon
 2011 Remote Sensing Data from Etowah's Mound A: Architecture and the Re-Creation of the Mississippian Tradition. *American Antiquity* 76(2):355-371.
- Kvamme, K.
 2003 Geophysical Surveys as Landscape Archaeology. *American Antiquity* 68(3):435-457.
- 2006 Magnetometry: Nature's Gift to Archaeology. In *Remote Sensing in Archaeology: An Explicitly North American Perspective*, edited by J. K. Johnson, pp. 205-234. University of Alabama Press, Tuscaloosa.
- Loke, M. H.
 2010 *Electrical Imaging Surveys for Environmental and Engineering Studies*. Universiti Sains Malaysia, Penang.

Mavko, G., T. Mukerji, and J. Dvorkin.

1998 *The Rock Physics Handbook: Tools for Seismic Analysis in Porous Media*. Cambridge University Press, Cambridge.

McKinnon, D. P.

2009 Exploring Settlement Patterning at a Premier Caddo Mound Site in the Red River Great Bend Region. *Southeastern Archaeology* 28(2): 248-258.

Nuzzo, L., G. Leucci, and S. Gri

2009 GPR, ERT and Magnetic Investigations Inside the Martyrium of St Philip, Hierapolis, Turkey. *Archaeological Prospection* 16(3):177–192. DOI: 10.1002/arp.364

Reynolds, J. M.

1997 *An Introduction to Applied and Environment Geophysics*. John Wiley and Sons, Ltd. New York.

Smekalova, T. N., O. Voss, and S. L. Smekalov

2005 *Magnetic Survey in Archaeology*. Publishing House of Polytechnic University, St. Petersburg, Russia.

Thompson, V. D. and T. J. Pluckhahn

2010 History, Complex Hunter-gatherers, and the Mounds and Monuments of Crystal River, Florida, USA: A Geophysical Perspective. *The Journal of Island and Coastal Archaeology* 5(1): 33-51.

Thompson, V. D., P. J. Arnold, T. J. Pluckhahn, and A. M. Vanderwarker

2011 Situating Remote Sensing in Anthropological Archaeology. *Archaeological Prospection* 18(3):195-213. DOI: 10.1002/arp.400

Tonkov, N. and M. H. Loke

2006 A Resistivity Survey of a Burial Mound in the ‘Valley of the Thracian Kings’ *Archaeological Prospection* 13(2):129–136. DOI: 10.1002/arp.273